

# 1 **Evaluating Simplifications of Subsurface Process**

## 2 **Representations for Field-scale Permafrost Hydrology Models**

3 Bo Gao, Ethan T. Coon

4 Environmental Sciences Division, Oak Ridge National Laboratory, Oak Ridge, Tennessee, USA

5 *Correspondence to:* Ethan T. Coon (coonet@ornl.gov)

6 **Abstract.** Permafrost degradation within a warming climate poses a significant environmental  
7 threat through both the permafrost carbon feedback and damage to human communities and  
8 infrastructure. Understanding this threat relies on better understanding and numerical  
9 representation of thermo-hydrological permafrost processes, and the subsequent accurate  
10 prediction of permafrost dynamics. All models include simplified assumptions, implying a tradeoff  
11 between model complexity and prediction accuracy. The main purpose of this work is to  
12 investigate this tradeoff when applying the following commonly made assumptions: (1) assuming  
13 equal density of ice and liquid water in frozen soil; (2) neglecting the effect of cryosuction in  
14 unsaturated freezing soil; and (3) neglecting advective heat transport during soil freezing and thaw.  
15 This study designed a set of 62 numerical experiments using the Advanced Terrestrial Simulator  
16 (ATS v1.2) to evaluate the effects of these choices on permafrost hydrological outputs, including  
17 both integrated and pointwise quantities. Simulations were conducted under different climate  
18 conditions and soil properties from three different sites in both column- and hillslope-scale  
19 configurations. Results showed that amongst the three physical assumptions, soil cryosuction is  
20 the most crucial yet commonly ignored process. Neglecting cryosuction, on average, can cause 10%  
21 ~ 20% error in predicting evaporation, 50% ~ 60% error in discharge, 10% ~ 30% error in thaw  
22 depth, and 10% ~ 30% error in soil temperature at 1 m beneath surface. The prediction error for  
23 subsurface temperature and water saturation is more obvious at hillslope scales due to the presence  
24 of lateral flux. By comparison, using equal ice-liquid density has a minor impact on most  
25 hydrological variables/metrics of interest, but significantly affects soil water saturation with an  
26 averaged 5% ~ 15% error. Neglecting advective heat transport presents the least error, 5% or even  
27 much lower, in most variables-metrics of interest for a large-scale general Arctic tundra system  
28 without apparent influence caused by localized groundwater flow, and can decrease the simulation  
29 time at hillslope scales by 40% ~ 80%. By challenging these commonly made assumptions, this

30 work provides permafrost hydrology scientists important context for [understanding the underlying](#)  
31 [physical processes, including allowing modelers to](#) better choose the appropriate process  
32 representation for a given modeling experiment.

33

34 **Copyright Statement.** This manuscript has been authored by UT- Battelle, LLC under Contract  
35 No. DE-AC05-00OR22725 with the U.S. Department of Energy. The United States Government  
36 retains and the publisher, by accepting the article for publication, acknowledges that the United  
37 States Government retains a non-exclusive, paid-up, irrevocable, world-wide license to publish, or  
38 reproduce the published form of this manuscript, or allow others to do so, for United States  
39 Government purposes. The Department of Energy will provide public access to these results of  
40 federally sponsored research in accordance with the DOE Public Access Plan  
41 (<http://energy.gov/downloads/doe-public-access-plan>).

## 42 **1 Introduction**

43 Permafrost describes a state of ground which stays frozen continuously over multiple years, which  
44 may cover an entire region (e.g., Arctic tundra) or occur in isolation (e.g., alpine top). From the  
45 perspective of scope, permafrost occupies approximately 23.9% (22.79 million km<sup>2</sup>) of the  
46 exposed land area of the northern hemisphere (Zhang et al., 2008), as well as alpine regions and  
47 Antarctica in the southern hemisphere. Permafrost areas store a vast amount of organic carbon, of  
48 which most is stored in perennially frozen soils (Hugelius et al., 2014). If the organic carbon is  
49 exposed due to permafrost thaw, it is likely to decay with microbial activity, releasing greenhouse  
50 gas to the atmosphere and exacerbating global warming. In Arctic tundra, permafrost also plays  
51 an important role in maintaining water, habitat of wildlife, landscape, and infrastructure (Berteaux  
52 et al., 2017; Dearborn et al., 2021; Hjort et al., 2018; Sugimoto et al., 2002). Permafrost  
53 degradation may cause significant damage to the local ecosystem, reshape the surface and  
54 subsurface hydrology, and eventually influence the global biosphere (Cheng and Wu, 2007;  
55 Jorgenson et al., 2001; Tesi et al., 2016; Walvoord and Kurylyk, 2016). Therefore, the occurrent  
56 and potential impacts motivate the development of computational models with the goal of better  
57 understanding the thermal and hydrological processes in permafrost regions, and consequently to  
58 predict permafrost thaw more accurately.

59 Simulating soil freezing and thaw processes is a challenging task that incorporates mass and energy

60 transfer among atmosphere, snowpack, land surface (perhaps with free water), and a variably  
61 saturated subsurface. Several hydrological models with different complexity and applicable scales  
62 have been developed to investigate the complicated interactions. Reviews of permafrost models  
63 based on empirical and physical representations using analytical and numerical solutions can be  
64 found in (Bui et al., 2020; Dall’Amico et al., 2011; Grenier et al., 2018; Jan et al., 2020; Kurylyk  
65 et al., 2014; Kurylyk and Watanabe, 2013; Riseborough et al., 2008). Process-rich models which  
66 aim to predict permafrost change through direct simulation of mass and energy transport, such as  
67 the Advanced Terrestrial Simulator (ATS; Painter et al., 2016), GEOtop (Endrizzi et al., 2014),  
68 CryoGrid 3 (Westermann et al., 2016), PFLOTRAN-ICE (Karra et al., 2014), and SUTRA-ICE  
69 (McKenzie et al., 2007), have been demonstrated to describe thermal permafrost hydrology under  
70 various climate conditions. Nominally, representing more physical process complexity should  
71 improve predictions of permafrost change, but the degree to which each process affects metrics of  
72 permafrost hydrology is highly uncertain and likely differs by scale. [Philosophically, models  
73 provide a useful tool precisely because they allow counterfactual experiments where processes are  
74 simplified to understand the relative importance of that process;](#) thus, [challenging](#) assumptions  
75 [about process](#) simplifications are a significant part of [both general process understanding,  
76 benefiting the permafrost hydrology community writ large, and](#) model [representations, benefiting  
77 the community of model developers and users.](#)

78 Even in the most process-rich models of permafrost change, three such physical simplifications  
79 are often made: representing water at constant density (thereby neglecting the expansion of ice  
80 relative to liquid water), neglecting cryosuction of water in unsaturated, partially frozen soils, and  
81 neglecting advective heat transport.

82 First, because of the lower density of ice than liquid water, freezing water must expand the volume  
83 of the porous media, push liquid water into nearby volume, or otherwise expand the volume  
84 occupied by that water. As [all-most](#) of the current set of models operate under the assumption of a  
85 rigid solid matrix and thus the absence of mechanical equations describing matrix deformation or  
86 frost heave, including this expansion typically results in large pressures that must be offset by grain  
87 compressibility or another mechanism. Therefore, the densities of ice and liquid water are  
88 frequently assumed equal (e.g., Dall’Amico et al., 2011; Devoie and Craig, 2020; Weismüller et  
89 al., 2011). It is uncertain whether this simplification affects predictions of permafrost change and  
90 thermal hydrology.

91 Second, cryosuction describes the redistribution of water in partially frozen, unsaturated soils  
92 caused by increased matric suction. At the interface of ice and liquid water, negative pressures  
93 result in the migration of liquid water toward the freezing front and the subsequent increase of ice  
94 content. Several approaches representing cryosuction in models are used (Dall’Amico et al., 2011;  
95 Noh et al., 2012; Painter and Karra, 2014; Stuurop et al., 2021), either in an empirical form or  
96 physically derived from the generalized Clapeyron equation. Other process-rich models have  
97 ignored cryosuction entirely (McKenzie et al., 2007; Viterbo et al., 1999). Dall’Amico et al. (2011),  
98 Painter (2011) and Painter and Karra (2014) evaluated their respective Clapeyron equation based  
99 cryosuction models in soil column freezing simulations and presented a good match between  
100 simulations and laboratory experiments in total water content (liquid and ice). Recently, Stuurop  
101 et al. (2021) applied an empirical expression, a physics-based expression, and no cryosuction in  
102 simulating soil column freezing process. They compared the simulated results with observations  
103 from laboratory experiments. This comparison demonstrated minor differences between empirical  
104 and Clapeyron-based cryosuction expressions, but the simulation without cryosuction cannot  
105 predict the distribution of total water content in a laboratory-scale soil column. To our knowledge,  
106 there is still no literature showing the effect of cryosuction on plot-scale permafrost predictions.

107 Third, heat transport in process-rich models is described using an energy conservation equation,  
108 mainly including heat conduction, latent heat exchange, and heat advection. From a continuum-  
109 scale perspective, conductive heat transport is expressed in the form of a diffusive term based  
110 on Fourier's law. Latent heat exchange accompanies phase change which alters the system enthalpy.  
111 Advective heat transport describes the energy exchange caused by the flow of liquid water driven  
112 by a hydraulic gradient (i.e., forced convection), which is expressed through an advective term in  
113 energy balance equations. Additionally, other mechanisms that control heat transport, such as  
114 water vapor movement, thermal dispersion, etc., are neglected by nearly all models of permafrost  
115 and are not considered here. ~~Among these heat transport mechanisms, it is commonly recognized~~  
116 ~~that heat conduction predominates heat transport in the subsurface (Nixon, 1975). However, there~~  
117 ~~are also~~ Several studies have demonstrated the importance of advective heat transport in  
118 permafrost hydrology through field observation analysis or modeling comparison. Such situations  
119 where advective heat transport makes important contributions roughly fall into three categories.  
120 The first centers on the development of taliks beneath lakes, ponds, topographic depressions, or  
121 other discontinuous permafrost effects (e.g., Dagenais et al., 2020; Liu et al., 2022; Luethi et al.,

122 2017; McKenzie and Voss, 2013; Rowland et al., 2011). The second focuses on microtopographic  
123 features that focus significant amount of water through small areas. This includes both low-center  
124 ice wedge polygons associated with the formation of thermokarst ponds (e.g., Abolt et al., 2020;  
125 Harp et al., 2021) and thermo-erosion gullies (e.g., Fortier et al., 2007; Godin et al., 2014). In these  
126 cases, large, focused flows across small spatial scales allow advective heat transport to dominate.  
127 The last category includes those studying the construction and maintenance of infrastructure  
128 influenced by groundwater flow (e.g., Chen et al., 2020). Thus, these studies focus on either  
129 location-specific or scale-limited problems. As McKenzie and Voss (2013) stated, whether heat  
130 advection outweighs heat conduction depends on soil permeability, topography, and groundwater  
131 availability. Relative to these special cases at small scales, we are more interested in to what extent  
132 advective heat transport associated with liquid water flow contributes to permafrost hydrologic  
133 change in a hillslope-scale or larger Arctic system. The Arctic systems, discussed hereinafter in  
134 this paper, refer to those with negligible influence caused by localized groundwater flow features  
135 as the three categories mentioned above.

136 To clarify the significant differences in model representations of permafrost, we investigate the  
137 influence of including or not including these processes on permafrost change at plot-to-hillslope  
138 scales. ~~We take the advantage of the flexibility offered by ATS to express multiple options of~~  
139 ~~process representation to implement this study in numerical experiments.~~ For ice density, we  
140 compare simulations with and without differences in ice density relative to water density; for  
141 cryosuction, we compare simulations using a Clapyron equation-based expression and excluding  
142 the cryosuction effect; and for heat transport, we compare simulations including or neglecting  
143 advective heat transport. All comparisons are carried out across a range of Arctic climate  
144 conditions and soil properties from three different sites. Both 1D soil-column-scale and 2D  
145 hillslope-scale models are considered, in which varying hillslope geometries (i.e.,  
146 convergent/divergent hillslope) and aspects (i.e., north/south) are included. ~~The aim of this study~~  
147 ~~is to provide permafrost hydrology modelers with crucial comparisons for better choosing a model~~  
148 ~~representation for a given study and better understanding permafrost physics by formally~~  
149 ~~considering the tradeoff between model complexity, accuracy, and, at least for one code,~~  
150 ~~performance.~~ The aim of this study is to provide better understanding of physical processes to  
151 permafrost hydrologists in general; and to offer some concrete insights to the model users and  
152 developers working on the process-rich models with similar theories and equation basis.

## 153 **2 Theory**

154 The Advanced Terrestrial Simulator (ATS v1.2) (Coon et al., 2020) configured in permafrost mode  
155 (Jan et al., 2018, 2020; Painter et al., 2016) was used to implement all numerical experiments in  
156 this study. ATS is a process-rich code developed for simulating integrated surface and subsurface  
157 hydrological processes, specifically capable of permafrost applications. It has been shown to  
158 successfully compare to observations of seasonal soil freezing and thaw processes at different  
159 scales. This includes 1D models of vertical energy transport typical of large-scale flatter regions  
160 (Atchley et al., 2015), and 2D models admitting lateral flow and transport in Arctic fens (Sjöberg  
161 et al., 2016), and polygonal ground (Jan et al., 2020).

162 The permafrost configuration of ATS comprises coupled water flow and energy transfer within  
163 variably saturated soils and at land surfaces, a surface energy balance model describing thermal  
164 processes in snow, and a snow distribution module for surface microtopography (Painter et al.,  
165 2016). The subsurface system solves a three-phase (liquid, ice, gas), two-component (water vapor,  
166 air) Richards-type mass balance equation with Darcy's law and an advection-~~diffusion-conduction~~  
167 energy balance equation. The surface system includes an overland flow model with diffusion wave  
168 approximation, and an energy balance equation with an introduced temperature-dependent factor  
169 describing the effect of surface water freezing. The subsurface system and surface system are  
170 coupled through the continuity of pressure, temperature, and the corresponding fluxes by  
171 incorporating the surface equations as boundary conditions of the subsurface equations (Coon et  
172 al., 2020). The evolution of a snowpack and its effect on the surface energy balance is described  
173 using an energy balance approach based on a subgrid model concept that includes all major heat  
174 fluxes at the land surface. For a more detailed description of the permafrost configuration and  
175 implementation in ATS, as well as key mathematical equations, the reader is referred to Painter et  
176 al. (2016). Changes in this “most complex” model of permafrost hydrology are enabled by the  
177 Arcos multiphysics library leveraged in ATS; this allows the precise model physics to be specified  
178 and configured at runtime through the use of a dependency graph describing swappable  
179 components in the model physics (Coon et al., 2016).

### 180 **2.1 Ice density**

181 The density of ice ( $\text{kg/m}^3$ ) is represented as a Taylor series expansion in both temperature and  
182 pressure:

183  $\rho_i = [a + (b + c\Delta T) \times \Delta T] \times (1 + \alpha\Delta p)$  (1)

184 and the density of liquid water (kg/m<sup>3</sup>) is represented as:

185  $\rho_l = [a + (b + (c + d\Delta T) \times \Delta T) \times \Delta T] \times (1 + \alpha\Delta p)$  (2)

186 where  $\Delta T = T - 273.15$ ,  $\Delta p = p_l - 1e5$ ,  $T$  and  $p_l$  are temperature (K) and liquid pressure (>101325

187 Pa), respectively; and  $a, b, c, d, \alpha$  are constant coefficients, listed in Table 1. Under conditions of

188 equal density, we assume  $\rho_i = \rho_l$ .

189

**Table 1 Coefficients in density of ice and liquid**

	$a$	$b$	$c$	$d$	$\alpha$
$\rho_i$	916.724	-0.147143	-2.38e-4	–	1.0e-10
$\rho_l$	999.915	0.0416516	-1.01e-2	2.06e-4	5.0e-10

190 **2.2 Cryosuction**

191 Several models are available in the literature describing the relationship between unfrozen water  
 192 content and temperature or matric suction (e.g., Ren et al., 2017; Stuurup et al., 2021), which is  
 193 also termed the soil freezing characteristic curve. These models are either associated with  
 194 temperature empirically or related to the soil water retention curve through the Clapeyron equation.  
 195 The latter approach normally incorporates the soil cryosuction process, while the former does not.  
 196 Painter and Karra (2014) proposed a physics-based constitutive model which relates the soil  
 197 unfrozen water content with the van Genuchten model (van Genuchten, 1980) relationship for  
 198 phase partitioning of water in frozen soils based on the Clapeyron equation and Van Genuchten  
 199 model (Van Genuchten, 1980):

200 
$$s_i = \begin{cases} S_*(-\beta\rho_l L_f \vartheta), \vartheta < \vartheta_f \\ S_*(p_g - p_l), \vartheta \geq \vartheta_f \end{cases}, \vartheta = \frac{T(K)-273.15}{273.15}, \vartheta_f = -\frac{\psi_*(1-s_g)}{\beta L_f \rho_l}$$
 (3)

201  $s_i = 1 - s_l/S_*(p_g - p_l)$

201 where  $s_n$  is the saturation of  $n$ -phase and the subscripts  $n = 1, i, g$  are liquid, ice, and gas phases,  
 202 respectively;  $\beta$  is a coefficient;  $L_f$  is the heat fusion of ice;  $p_n$  ( $n = 1, g$ ) is the pressure of  $n$ -phase;  
 203  $S_*$  is the Van Genuchten model. This physically derived formulation can describe the change of  
 204 matric suction in the frozen zone due to the change of ice content, and thus has the capacity to  
 205 represent cryosuction.

206 Alternatively, the unfrozen water content can be also expressed as a single-variable function  
 207 dependent on sub-freezing temperature for a given soil, ignoring the effect of cryosuction, such as  
 208 the following (McKenzie et al., 2007): ~~to exclude the effect of cryosuction in this study, we used~~



209 ~~the Van Genuchten model to determine the total water content, including liquid water and ice. The~~  
 210 ~~liquid water content is achieved by an empirical relationship (soil freezing characteristic curve)~~  
 211 ~~which describes that the liquid water content only relates to temperature through an exponent~~  
 212 ~~function (McKenzie et al., 2007).~~

$$213 \quad s_l = s_r + (s_{\text{sat}} - s_r) \exp \left[ - \left( \frac{T(\text{K}) - 273.15}{\omega} \right)^2 \right] \quad (4)$$

$$s_i = S_* (p_g - p_l) - s_l$$

214 where  $s_r$ ,  $s_{\text{sat}}$  are saturations of liquid water at residual and saturated conditions, respectively;  $\omega$  is  
 215 a constant coefficient. In this case, the van Genuchten model was used to determine the total water  
 216 content, including liquid water and ice.

### 217 2.22.3 Advective heat transport

218 The energy conservation equation of the subsurface system is given by:

$$219 \quad \frac{\partial}{\partial t} [\phi \sum_{n=l,i,g} (\rho_n s_n u_n) + (1 - \phi) c_{v,\text{soil}} T] + \underbrace{\nabla \cdot (\rho_l h_l \mathbf{V}_l)}_{\text{advective heat}} - \underbrace{\nabla \cdot (\kappa_e \nabla T)}_{\text{conductive heat}} = Q_E \quad (5)$$

220 where  $\phi$  is porosity;  $u_n$  is the specific internal energy of phase ( $n \in \{l, i, g\}$ );  $c_{v,\text{soil}}$  ( $\text{J m}^{-3} \text{K}^{-1}$ ) is  
 221 the volumetric heat capacity of the soil grains. The second and third terms represent the advective  
 222 and conductive heat transport in the subsurface, in which  $h_l$  ( $\text{J/mol}$ ) is the specific enthalpy of  
 223 liquid;  $\mathbf{V}_l$  ( $\text{m/s}$ ) is the velocity vector of liquid water determined by Darcy's law; and  $\kappa_e$  ( $\text{W m}^{-1}$   
 224  $\text{K}^{-1}$ ) is the effective thermal conductivity of the bulk material including soil, air, liquid water, and  
 225 ice.  $Q_E$  is the sum of all thermal energy sources ( $\text{W/m}^3$ ).

226 Similarly, the energy balance equation of the surface system is:

$$227 \quad \frac{\partial}{\partial t} \{ [\chi \rho_l u_l + (1 - \chi) \rho_i u_i] \delta_w \} + \underbrace{\nabla \cdot (h_l \chi \rho_l \delta_w \mathbf{U}_w)}_{\text{advective heat}} - \underbrace{\nabla \cdot \{ [\chi \kappa_l + (1 - \chi) \kappa_i] \delta_w \nabla T \}}_{\text{conductive heat}} = Q_{\text{net}} \quad (6)$$

228 in which  $\chi$  is the unfrozen fraction of surface determined by surface temperature;  $\delta_w$  is ponded  
 229 depth ( $\text{m}$ );  $\mathbf{U}_w$  ( $\text{m/s}$ ) is the velocity vector of liquid water on the surface determined by the  
 230 diffusion-wave approximated St. Venant equations (Gottardi and Venutelli, 1993) and Manning  
 231 equation (Wasantha Lal, 1998);  $\kappa_n$  ( $\text{W m}^{-1} \text{K}^{-1}$ ) is the thermal conductivity of  $n$ -phase ( $n = l, i$ );  
 232  $Q_{\text{net}}$  ( $\text{W/m}^3$ ) is the net thermal energy into and out of ground surface, including that from solar  
 233 radiation, rain and snow melt, water loss by evaporation and to the subsurface, and conductive and  
 234 advected heat transport to/from the subsurface. The second and third terms represent the (lateral)  
 235 advective and conductive heat transport that occur across the land surface.



### 236 **3 Methods**

237 To evaluate the impact of representation of ice density, cryosuction, and advective heat transport  
238 in permafrost modeling under different climate conditions and soil properties, we selected three  
239 sites for their variance in climactic condition: Utqiagvik (Barrow Environmental Observatory,  
240 71.3225° N, 156.6231° W), the headwaters of the Sagavanirktok (Sag) River (68.251° N, 149.092°  
241 W), and the Teller Road Mile Marker 27 site on the Seward Peninsula (64.73° N, 165.95° W) in  
242 Alaska. The simulated hydrological outputs for each site are compared in both column and  
243 hillslope scenarios. Column scenarios represent expansive flat regions typical of the Arctic coastal  
244 plains dominated by vertical infiltration and heat transport, and hillslope scenarios are  
245 representative of the headwater, hilly terrain typical of the more inland permafrost.

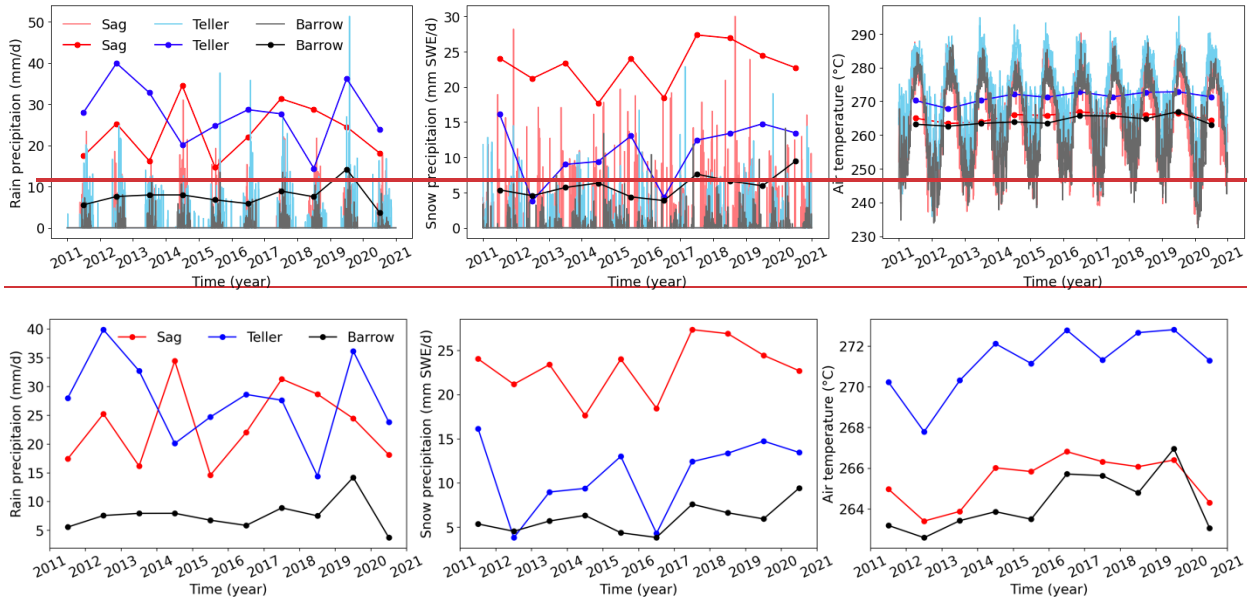
246 In hillslope scenarios, hillslopes with northern and southern aspects are considered to investigate  
247 physics representation comparisons under the same climate and soil condition (i.e., at a given site)  
248 but different solar radiation incidence. Furthermore, hillslopes with both convergent and divergent  
249 geometries are included to compare the sensitivity of simulated discharge on process  
250 representation. These scenarios can incorporate many types of Arctic systems at the described plot-  
251 to-regional scales, but explicitly ignore the effects of microtopography or other local-scale  
252 focusing mechanisms such as water tracts or thermo-erosion gullies. The objective is to reach a  
253 conclusion on the influence of the three physics representations that can be widely applicable in  
254 many Arctic systems.

#### 255 **3.1 Field data description**

256 For each site, data used in each simulation comprises meteorological forcing datasets for the period  
257 2011-2020, averaged wind speed, and soil properties.

258 Meteorological forcing datasets are taken from the Daymet version 4 dataset (Thornton et al., 2020),  
259 which provides observation-based, daily averaged weather variables through statistical modeling  
260 techniques at 1 km spatial resolution (Thornton et al., 2021). Variables that are used in simulations  
261 include daily average air temperature (calculated as the mean of Daymet's daily minimum and  
262 maximum values), relative humidity (calculated from air temperature and Daymet's vapor  
263 pressure), incoming shortwave radiation ( $W/m^2$ ) (calculated as a product of Daymet's daylit  
264 incoming radiation and daylength), and total precipitation (m/s), which is split into snow and rain  
265 based upon the air temperature. Figure 1 illustrates the precipitation of rain, snow, and air

266 temperature ~~in~~at the three sites from 2011 to 2020, where the points represent the corresponding  
 267 averaged values per year. In terms of the forcing conditions, the annual rainfall of the Sag and  
 268 Teller sites range between 20 and 40 mm/d over the ten years, more than twice the rainfall typical  
 269 of the Barrow site. In addition, Sag has a significantly larger amount of snow every year that is  
 270 over double ~~of~~ that at the Teller site and almost five times larger compared to the Barrow site. For  
 271 the air temperature, Sag and Barrow are similar and colder than Teller by 7-8 degrees. In general,  
 272 the Barrow site is dry and cold, the Sag site is wet and cold, and the Teller site is wet and warm.

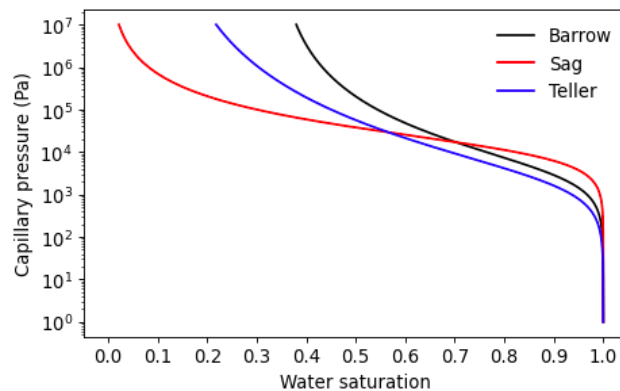


273  
 274  
 275 **Figure 1 Precipitation and air temperature of site Barrow, Sag, and Teller from year 2011 to 2020**

276 In addition to the time series of forcing data from Daymet, we used an average wind speed for  
 277 each site. For Barrow and Teller, the average wind speed was estimated from the measurement  
 278 taken by the Next-Generation Ecosystem Experiments (NGEE) Arctic project. At Barrow, the  
 279 measurement was taken at area A (71.2815° N, 156.6108 ° W) at the height of 1.3 meters above  
 280 surface (Hinzman et al., 2014). At Teller, the measurement at 3.8 m above the surface of a lower  
 281 level of the watershed (Busey et al., 2017) was used. For Sag, the average wind speed was  
 282 estimated based on the measurement at the Toolik Lake field site (near to Sag River) at the height  
 283 of 3.1 m above surface, which is accessible through the National Ecological Observatory Network  
 284 (NEON, 2021).

285 The soil properties of Barrow, Sag, and Teller, including porosity, permeability, Van Genuchten  
 286 parameters, and thermal conductivity parameters, were chosen from previous modeling studies at  
 287 these sites (Atchley et al., 2015; Jafarov et al., 2018; O'Connor et al., 2020), see (Table 2). Roughly,

288 the soil profile of each site is composed of two materials: the top organic-rich layer comprising  
289 mosses, peats, and other organic rich soils measuring approximately 10-30 cm thick, and the  
290 principal mineral soil. There is minor difference in thermal conductivity parameters among the  
291 three sites, and soil permeability is also at the same order of magnitude. The soil-water  
292 characteristic curve (SWCC) of the principal mineral soil of Barrow, Sag, and Teller, shown in  
293 Figure 2, indicates that the soil properties ~~between at~~ Barrow and Teller ~~is-are~~ relatively similar,  
294 while Sag differs from the other two with a relatively flat SWCC.



295  
296 **Figure 2 Soil-water characteristic curve (SWCC) of soil in Barrow, Sag, and Teller**

297 Usually, at the hillslope scale, the thickness of organic layers of a watershed varies from the toe-  
298 slope, through a steeper mid-hill, up to the flat top. Typically, thicker organic layers may exist at  
299 the top and bottom compared to the mid-hillslope. The low thermal conductivity of organic layers  
300 can impede the heat transport between the air and the underlying mineral soil, resulting in varying  
301 thaw depth (or permafrost table depth) along a hillslope, which has been observed at ~~the site~~ Teller  
302 (Jafarov et al., 2018). In this paper, hillslope meshes were constructed following this observation  
303 so that the organic layers are thicker at the top and bottom of a hillslope, as described in the next  
304 section.

### 305 **3.2 Mesh design and material properties**

306 The comparison of different physics representations was conducted in both column and hillslope  
307 scenarios.

308 The column model was designed as a one-dimensional, 50 m deep domain. The column domain  
309 was discretized into 78 cells with gradually increasing cell thickness, starting from 2 cm at the soil  
310 surface to 2 m at the bottom of the domain. We assigned different material properties to the cells  
311 to represent different soil layers. A column domain is divided into three layers, and the thickness

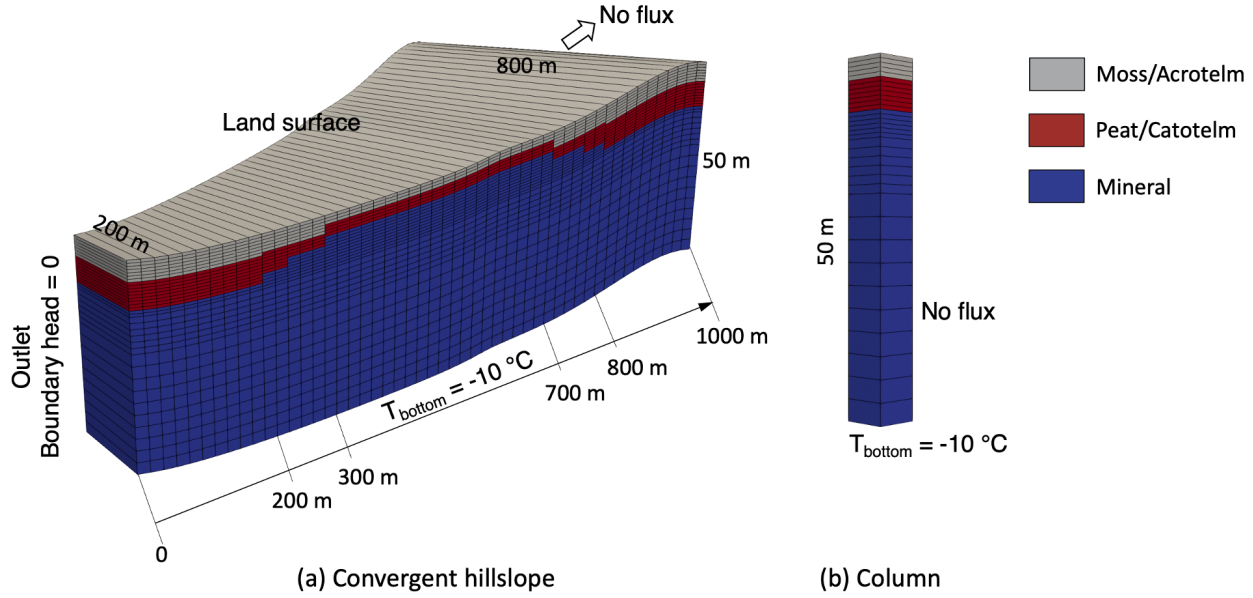
312 of each layer was designed differently among the three sites according to geological observations  
 313 (Jan et al., 2020; O'Connor et al., 2020; NGEE-Arctic). Specifically, from top to bottom, the three  
 314 layers of the Barrow soil column are 2 cm-thick moss, 8 cm-thick peat, and mineral; for Teller, the  
 315 soil column consists of a 4 cm moss layer, a 22 cm peat layer, and mineral; and the three layers of  
 316 the Sag soil column are acrotelm, catotelm, with thickness of 10 cm and 14 cm, respectively, and  
 317 the remainder mineral. The soil properties of each layer at three sites are listed in Table 2.

318 **Table 2 Soil properties of three soil layers of all sites used in this paper**

Site	Barrow			Sag			Teller		
Layers	moss	peat	mineral	acrotelm	catotelm	mineral	moss	peat	mineral
Porosity	0.9	0.876	0.596	0.878	0.796	0.457	0.9	0.55	0.45
Permeability (m <sup>2</sup> )	1.7e-11	9.38e-12	6e-13	2.64e-10	9.63e-12	3.98e-13	5e-11	5e-12	2e-13
VG $\alpha$ (Pa <sup>-1</sup> )	2.3e-3	9.5e-4	3.3e-4	7.93e-4	1.75e-4	8.06e-5	2.35e-3	2.93e-4	5.45e-4
VG n	1.38	1.44	1.33	1.405	1.566	1.571	1.38	1.269	1.236
Residual saturation	0.056	0.388	0.334	0.0073	0.0662	0.	0.1	0.	0.1
Thermal conductivity, unfrozen (Wm <sup>-1</sup> K <sup>-1</sup> )	0.446	0.427	0.788	0.519	0.630	1.309	0.57	0.67	1
Thermal conductivity, dry (Wm <sup>-1</sup> K <sup>-1</sup> )	0.024	0.025	0.104	0.066	0.086	0.265	0.07	0.07	0.29

319

320 In the hillslope scenario, we designed the mesh based on observations at Teller to represent a  
 321 generalized, varying-thickness low Arctic hillslope. A hillslope mesh was created first by  
 322 generating a pseudo-2D surface mesh with 50 cells and then extruding the 2D mesh downward by  
 323 50 m. The pseudo-2D surface was designed in a trapezoidal shape with a single, variable-width  
 324 cell in the cross-slope direction to represent convergent/divergent hillslopes, the short and long  
 325 sides of which are 200 m and 800 m, respectively (see Figure 3). Vertically, from surface  
 326 downward, the grid size distribution was the same as the column mesh for each site. The domain  
 327 is also composed of three layers, same as the column, while the numbers of cells representing each  
 328 soil layer (i.e., soil layer thickness) are different along the hillslope. The thickness distribution of  
 329 the first two layers of each site is shown in Table 3. The third layer of a hillslope for all sites is the  
 330 principal mineral soil. Additionally, hillslope meshes with different aspects (i.e., north-facing,  
 331 south-facing) were also created.



332  
333 **Figure 3 Schematic domain mesh and soil layer partition: (a) example of a convergent hillslope domain, (b)**  
334 **column domain.**

335 **Table 3 Thickness distribution of the organic layers along hillslope for each site**

Site	Horizontal $x$ range (m)	Barrow layer thickness (cm)	Sag layer thickness (cm)	Teller layer thickness (cm)
Layer 1 Moss/Acrotelm	0 ~ 200	2	14	8
	300 ~ 700	2	6	4
	800 ~ 1000	2	14	8
Layer 2 Peat/Catotelm	0 ~ 200	12	18	22
	300 ~ 700	6	8	22
	800 ~ 1000	12	18	22

### 336 3.3 Model setup

337 To study how the representations of the three physical processes (i.e., ice expansion represented  
338 by density, cryosuction, and advective heat transport) affect simulated hydrological outputs at  
339 different scales and hillslope topography features, and under various forcing and soil conditions,  
340 62 model simulations were conducted, summarized in Table 4. To examine the validity of the  
341 assumption of equal density between ice and liquid water, we included cryosuction and advective  
342 heat transport in models. To investigate the role of cryosuction in permafrost modeling, we used  
343 different density, while neglecting advective heat transport to decrease the computation cost. Note  
344 that neglecting advective heat transport in these runs can reduce the effect of cryosuction on  
345 simulation predictions, as cryosuction moves water which would itself advect energy. To compare  
346 the difference between neglecting and including heat advection, we used different density  
347 expressions for ice and liquid, and included cryosuction. Particularly, in order to understand the

348 impact of advective heat transport on permafrost processes when soil is at its wettest, we designed  
 349 two extreme cases under the warm, wet conditions of the Teller site in which soil evaporation was  
 350 ~~factitiously-artificially~~ reduced. These runs were designed to maximize water flux and therefore  
 351 maximize the potential for advective heat transport to affect predictions.

352 **Table 4 Ensemble of models designed in this study**

To compare	Site	Scale	Geometry	Aspect	Remark
<ul style="list-style-type: none"> <li>• <math>\rho_i \neq \rho_l</math>, Eq. (1)</li> <li>• <math>\rho_i = \rho_l</math>, Eq. (2)</li> </ul>	Barrow Sag Teller	column	–	–	<ul style="list-style-type: none"> <li>• heat advection</li> <li>• cryosuction</li> </ul>
		hillslope	convergent	north south	
<ul style="list-style-type: none"> <li>• Include heat advection</li> <li>• Neglect heat advection</li> </ul>	Barrow Sag Teller	column	–	–	<ul style="list-style-type: none"> <li>• <math>\rho_i \neq \rho_l</math></li> <li>• cryosuction</li> </ul>
		hillslope	convergent	north south	
	Extreme case, Teller	hillslope	convergent	north	• reduced evaporation
<ul style="list-style-type: none"> <li>• Include cryosuction</li> <li>• Neglect cryosuction</li> </ul>	Barrow Sag Teller	column	–	–	<ul style="list-style-type: none"> <li>• <math>\rho_i \neq \rho_l</math></li> <li>• no heat advection</li> </ul>
		hillslope	convergent	north south	
			divergent	north south	

353  
 354 Prior to simulating all cases, two steps of initialization are carried out for each site. First, a column  
 355 model ~~initially above freezing temperature~~ with a given ~~initial~~ water table depth ~~and above 0 °C~~  
 356 ~~temperature~~ was frozen by setting the bottom temperature at a constant value of -10 °C until a  
 357 steady-state frozen soil column is formed. The initial water table depth is chosen to ensure that the  
 358 frozen column's water table, after accounting for expansion of ice, is just below the soil surface.  
 359 The pressure and temperature profiles of the frozen column were used as the initial conditions of  
 360 the second step initialization. Before proceeding, the observed forcing data (period of 2011-2020)  
 361 was averaged across the years to form a one-year, "typical" forcing year, which was then repeated  
 362 10 times. Using this typical forcing data and the solutions of the first step, we solved the column  
 363 model in a transient solution, calculating an annual cyclic steady state ~~and obtaining the pressure~~  
 364 ~~and temperature fields at the end of the 10<sup>th</sup> year~~. The final ~~pressure and temperature profile of the~~  
 365 ~~column at the end of the 10-year simulation state~~ was then ~~assigned to each column of the hillslope~~  
 366 ~~mesh used~~ as ~~the~~ initial condition in ~~the~~ formal simulations listed in Table 4. The temperature at  
 367 ~~the~~ bottom was constant at -10 °C.

### 368 3.4 Evaluation metrics

369 To fully assess the effect of representation of ice density, advective heat transport, and cryosuction  
370 in permafrost hydrology modeling, we used [the](#) root mean squared error (RMSE) and normalized  
371 Nash–Sutcliffe efficiency (NNSE) as performance metrics. RMSE has the same dimension as the  
372 corresponding variables, which can be used to evaluate the average absolute deviation from a  
373 benchmark, defined by:

$$374 \text{ RMSE} = \sqrt{\frac{\sum_{t=1}^N (x_t - y_t)^2}{N}} \quad (7)$$

375 where  $x_t$  and  $y_t$  are the two modeled datasets to compare from the initial time point ( $t = 1$ ) to the  
376 end ( $t = N$ ).

377 NNSE is a normalized dimensionless metric describing the relative relationship between an  
378 estimation and a reference, which is oftentimes used for evaluating hydrological models~~:-~~:

$$379 \text{ NNSE} = 1 / \left( 1 + \frac{\sum_{t=1}^N (x_t - y_t)^2}{\sum_{t=1}^N (x_t - \bar{x})^2} \right) \quad (8)$$

380 where the modeled results  $x_t$  (obtained without physics simplification) are considered as the  
381 benchmark, and  $\bar{x}$  is the mean value of the benchmark. A NNSE approaching 1 indicates perfect  
382 correspondence between two [groups of values in comparison-observations](#).

383 In addition, we also used [the](#) normalized mean absolute error (MAE) to quantify the percentage  
384 change of results obtained with simplified physics relative to full physical representations (see  
385 Section 4.4)~~:-~~:

$$386 \text{ Normalized MAE} = \frac{\sqrt{\sum_{t=1}^N |x_t - y_t| / N}}{\text{normalizing reference}} \times 100\% \quad (9)$$

387 Two normalizing references were selected considering different [modeled metrics of interest](#)~~model~~  
388 [output variables](#). For instance, in terms of temperature and saturation which fluctuate between two  
389 non-zero values, the annually averaged variation range was chosen as the reference~~:-~~:

$$390 \text{ Normalizing reference} = \frac{\sum_{\text{year}=1}^{\text{num of years}} (\text{maximum} - \text{minimum})}{\text{number of years}}$$

391 For [variables-a modeled metric](#) with zero as the smallest value, such as evaporation, discharge,  
392 and thaw depth, the corresponding average value was selected as the reference.

## 393 4 Results

394 This section compares simulated outputs over the period of 2011-2020 for the three physical~~s~~



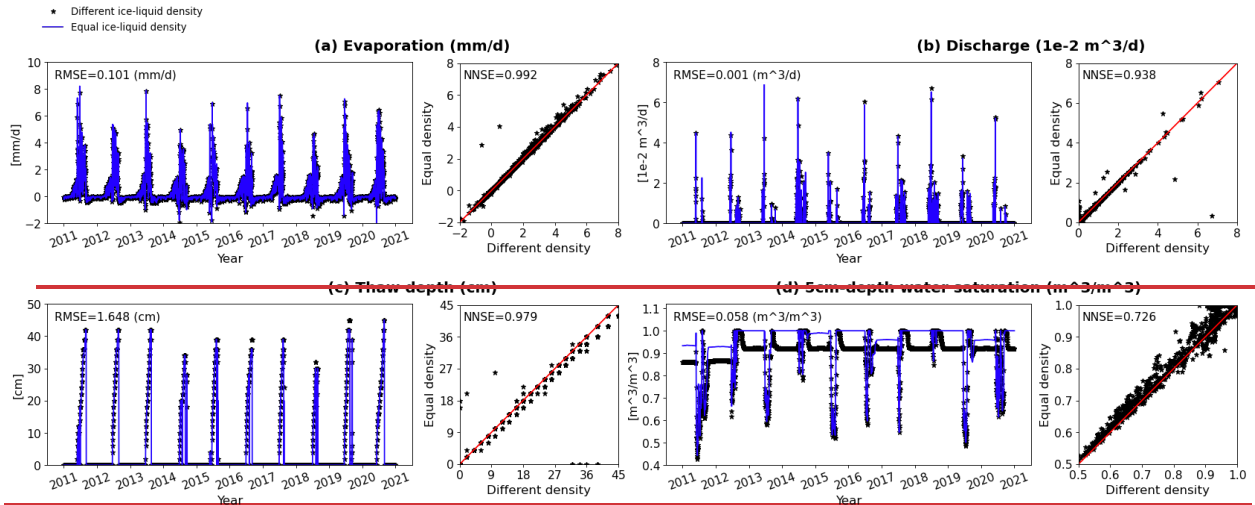
395 processes under different simulating conditions. We focus on the impact on integrated  
396 variablesmetrics, such as evaporation, discharge, averaged thaw depth, and depth-dependent  
397 variablesmetrics, such as temperature, and total water saturation (ice and liquid). For hillslope  
398 models, we chose five surface locations according to the slope geometry to collect simulated data,  
399 which were then averaged to obtain a single outcome for each variable-metric of interest.

#### 400 **4.1 Ice density**

401 To evaluate the representation of ice density on permafrost process simulation, we compared  
402 evaporation, discharge, thaw depth, and total water saturation between simulations using equal and  
403 different ice density expressions. Figure 4 and Figure 5 show an example of the comparison under  
404 conditions of Sag at column and hillslope scales, respectively. Results are compared in both time  
405 series and correlation.

406 Generally, at both column and hillslope scales, assuming equal density between ice and liquid has  
407 minor impacts on evaporation, discharge, and thaw depth over the 10-year simulation, except at a  
408 few deviated points as shown in the correlation figures. According to column-based models, the  
409 RMSEs of evaporation, discharge, and thaw depth are 0.101 mm/d, 0.001 m<sup>3</sup>/d, and 1.648 cm,  
410 respectively, one order of magnitude smaller than the values of the corresponding variablemetrics  
411 values. At the hillslope scale (see Figure 5) the south-facing divergent hillslope is selected to show  
412 modeling comparison on evaporation and thaw depth, in that they are potentially mostly affected  
413 when a hillslope has a south orientation and divergent geometry. Likewise, the north-facing  
414 convergent hillslope is chosen to compare discharge and water saturation from simulations with  
415 different density expressions. Even then, RMSEs of the three variables-metrics are 0.064 mm/d,  
416 111.073 m<sup>3</sup>/d, and 0.825 cm, respectively, two orders of magnitude smaller than the values of the  
417 corresponding variable-valuesmetrics at the hillslope scale. Besides, NNSEs of the three variables  
418 metrics output from both column and hillslope simulation are over 0.9, approaching 1 especially  
419 at the hillslope scale. Therefore, all indicate good performance of equal ice-liquid density  
420 assumption in predicting integrated variables-metrics and thaw depth. By comparison, the  
421 estimation of water saturation is relatively more affected by the density assumption during cold  
422 seasons within a year, as shown by Figure 4 (d) and Figure 5 (d). This is reasonable in that when  
423 water mainly exists in the form of ice, equal ice-liquid density assumption will overestimate the  
424 water content.

425

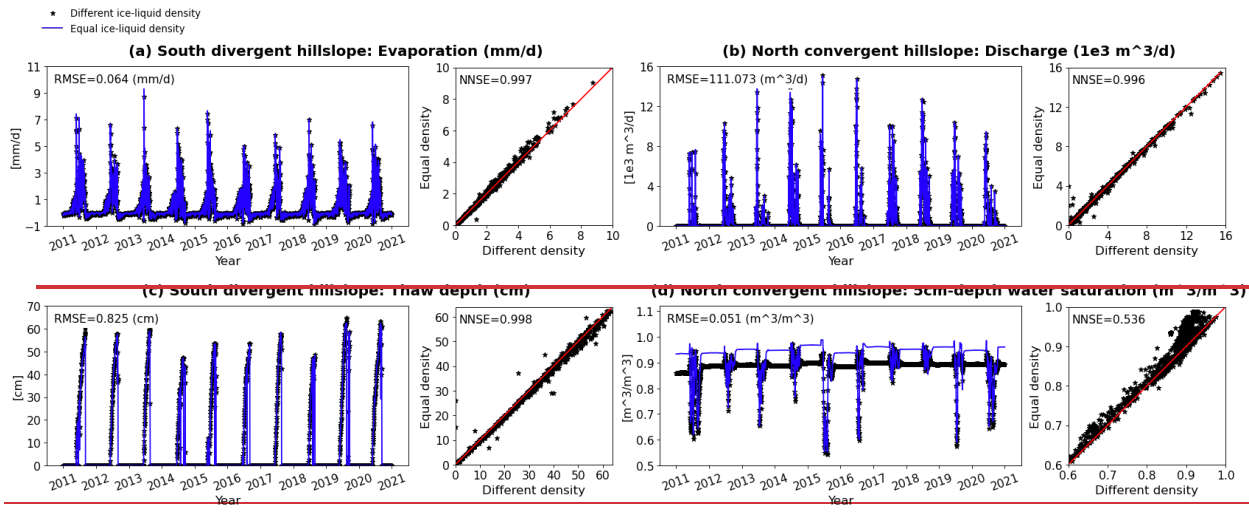


426

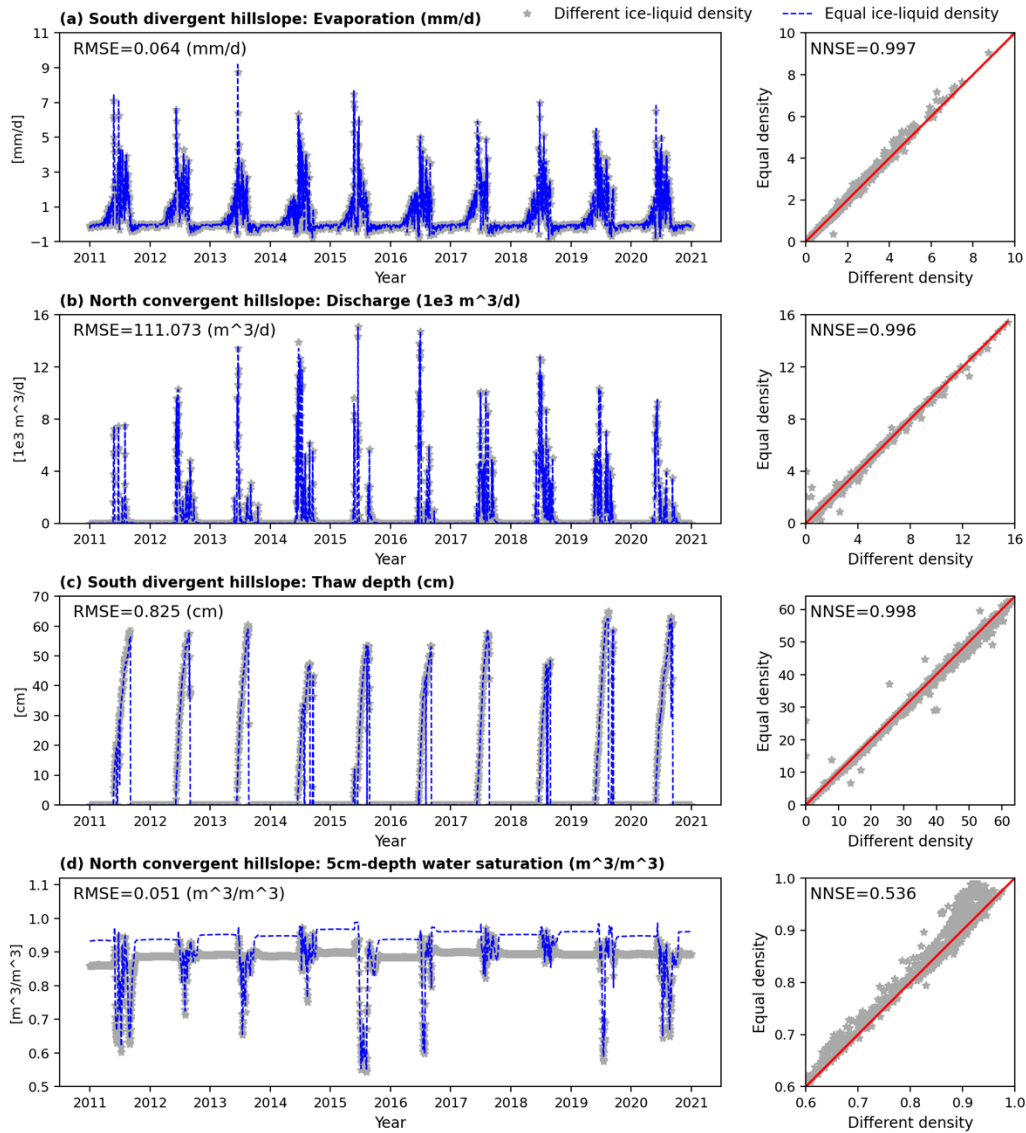
427

Figure 4 Comparison of column simulations between different and equal ice-liquid density under conditions

428 of Sag, in (a) evaporation, (b) discharge, (c) thaw depth, and (d) water saturation at 5 cm beneath surface  
 429 from year 2011 to 2020.



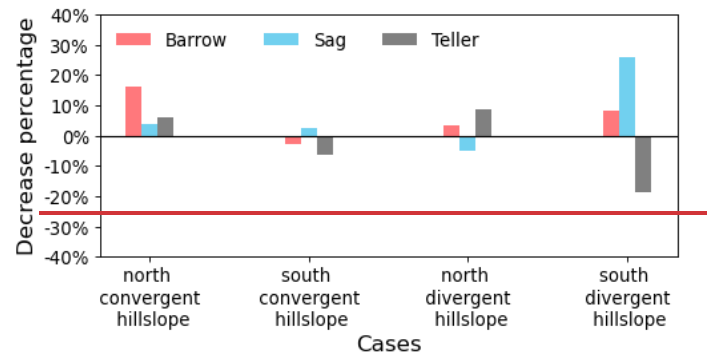
430



431  
 432 **Figure 5 Comparison of hillslope simulations between using different and equal ice-liquid density under**  
 433 **conditions of Sag, in (a) evaporation, (b) discharge, (c) thaw depth, and (d) water saturation at 5 cm beneath**  
 434 **surface from year 2011 to 2020.**

435 ~~In addition, we investigated how much the assumption of equal ice-liquid density can affect~~  
 436 ~~simulation time at hillslope scale. Using 10-year simulations with real ice density as references,~~  
 437 ~~the percentage change of time consumed after applying equal ice-liquid density was calculated and~~  
 438 ~~displayed in Figure 6. Overall, under the density assumption, it may take less time (positive~~  
 439 ~~percentage), but no more than 25% and on average lower than 10%. However, it may also increase~~  
 440 ~~computational time (negative percentage) mainly under wet conditions, such as at Sag and Teller.~~  
 441 ~~Thus, given a long-period large-scale modeling of permafrost freezing and thaw process, there is~~  
 442 ~~no consistent conclusion on whether equal ice-liquid density can ease computational cost. It~~

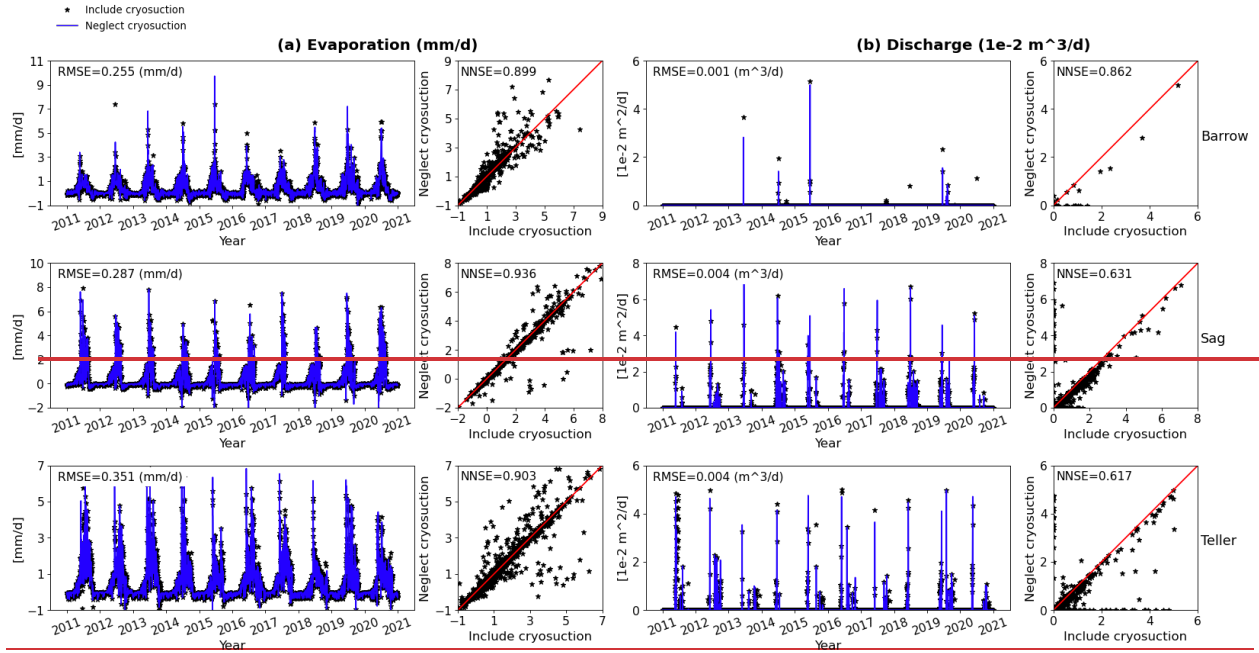
443 depends on both the weather conditions and soil properties.



444  
445 **Figure 6 Decreased percentage of simulation time under the assumption of equal ice liquid density compared**  
446 **to the real ice density representation for all hillslope scale simulations.**

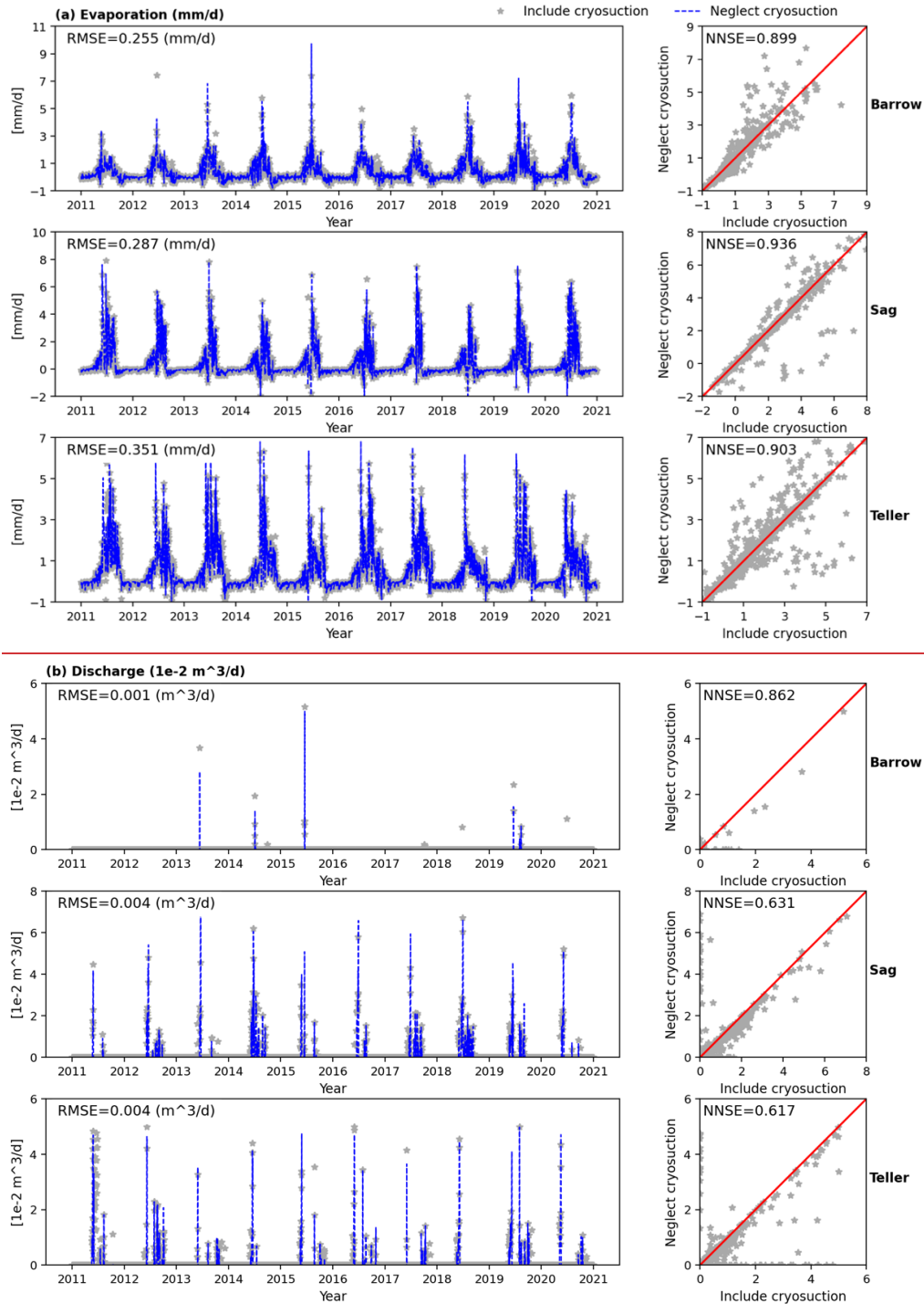
## 447 4.2 Cryosuction

448 To evaluate the effect of cryosuction on permafrost process predictions, we compared evaporation,  
449 discharge, thaw depth, total water saturation, and temperature obtained through simulations  
450 including and neglecting cryosuction. Figure 6 through Figure 8 illustrate column-scale  
451 comparisons of these variables-metrics under conditions at the three sites (Barrow, Sag, and Teller).  
452 Figure 6 presents the effect of excluding cryosuction on evaporation and discharge. The RMSE of  
453 evaporation from the three sites ranges between 0.25 mm/d and 0.35 mm/d, still one order of  
454 magnitude smaller than the common evaporation rate. Evaporation NNSEs of the three sites are  
455 around 0.9. For discharge, RMSEs are also one order of magnitude smaller than the average,  
456 whereas NNSEs fall between 0.6 and 0.9. Generally, cryosuction plays a more important role in  
457 predicting discharge compared to evaporation, especially under warm and wet climate conditions,  
458 such as Teller.



459

460



461

462 **Figure 6 Comparison of column simulations between including and neglecting cryosuction under conditions**  
463 **of Barrow, Sag, and Teller, in (a) evaporation, (b) discharge.**

464

Figure 7 shows the effect of cryosuction on column-scale simulated thaw depth and total water

465

saturation at 5 cm beneath the surface. Overall, neglecting cryosuction tends to underestimate the

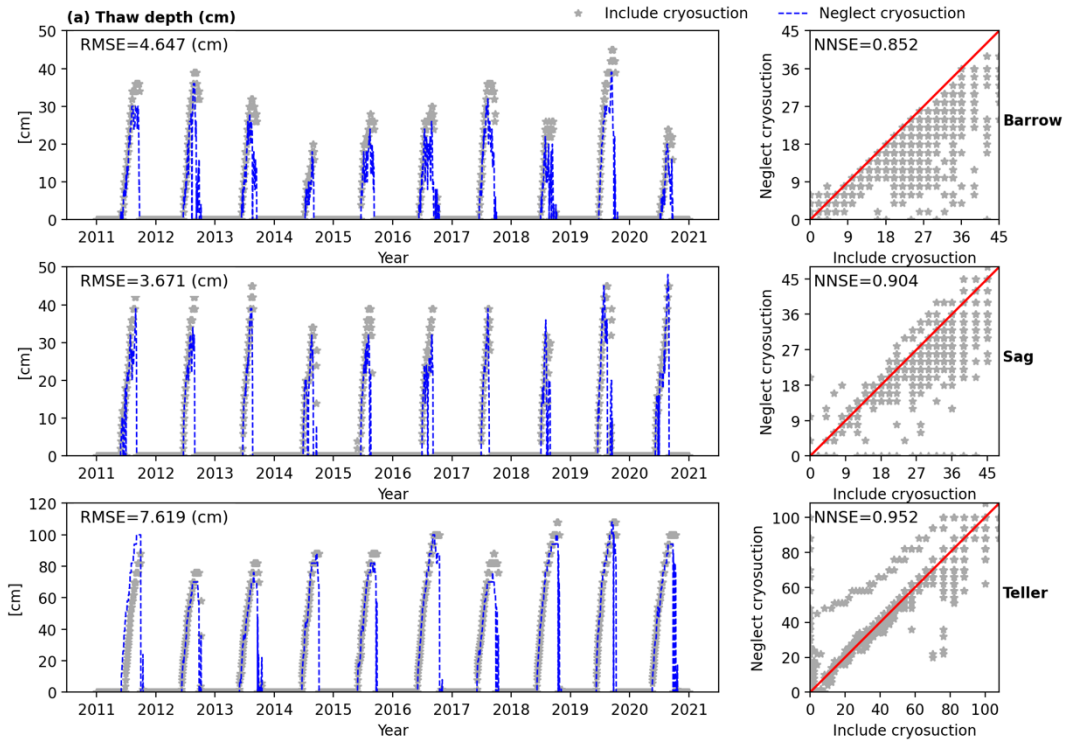
466

deepest thaw depth. As already mentioned, cryosuction, in essence, increases soil suction to attract

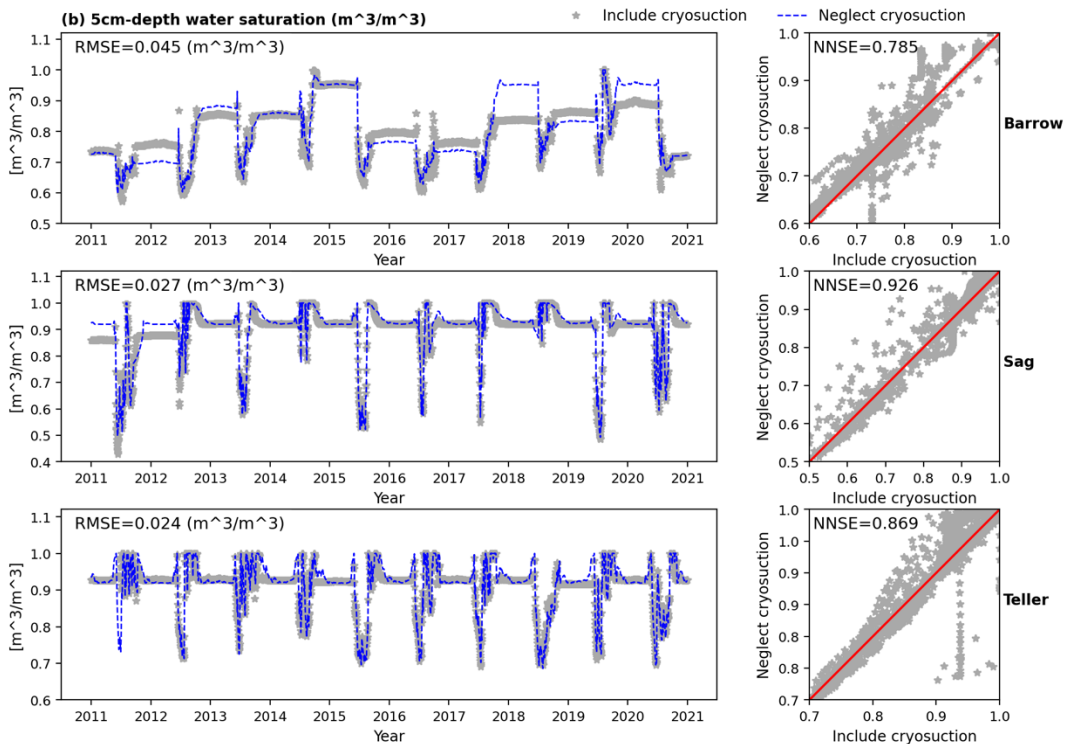


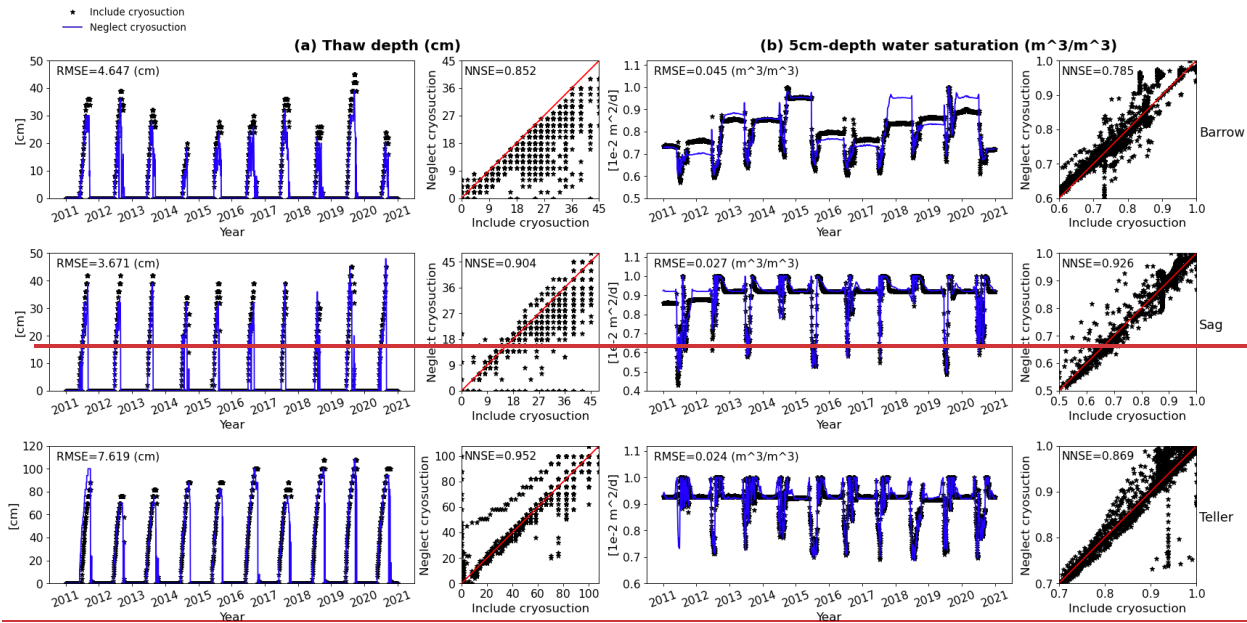
467 more liquid water moving towards the frozen front during soil freezing. Thus, the real active layer  
468 formed due to the existence of cryosuction should be thicker than the cases in which cryosuction  
469 is assumed unimportant. RMSEs of thaw depth in Figure 7 range from 3 cm to 8 cm. Though still  
470 one order of magnitude smaller than the average annual thaw depth, the estimation error due to  
471 neglecting cryosuction is most obvious in summer, especially at areas with cold temperature like  
472 Barrow. RMSEs of thaw depth range from 3 cm to 8 cm. Though still one order of magnitude  
473 smaller than the average annual thaw depth, the estimation error due to neglecting cryosuction is  
474 obvious in summer, especially at areas with cold temperature and low rainfall like Barrow. By  
475 comparison, at Teller, where the largest thaw depth is over double that of Barrow and Sag due to  
476 its higher temperature, soil cryosuction does not essentially affect thaw depth compared to the  
477 other two sites. Similarly, for the total water saturation, at Barrow, the effect of cryosuction is  
478 more clearly observed, not only during cold seasons as observed for density representation (section  
479 4.1), but also in summers. The reason why Barrow is more sensitive to the cryosuction process on  
480 predicting thaw depth and water content is determined by both soil properties and climate  
481 conditions. The soil at Barrow has larger suction and is able to hold more water (see Figure 2),  
482 providing the possibility for cryosuction to make contributions. Moreover, the principal difference  
483 between cryosuction and non-cryosuction representations is presented when the temperature is  
484 below the freezing point (see Eq.(3) and Eq.(4)). Compared to Sag and Teller, Barrow has lower  
485 annual average temperature (see Figure 1), making the effect of cryosuction more pronounced.

486



487



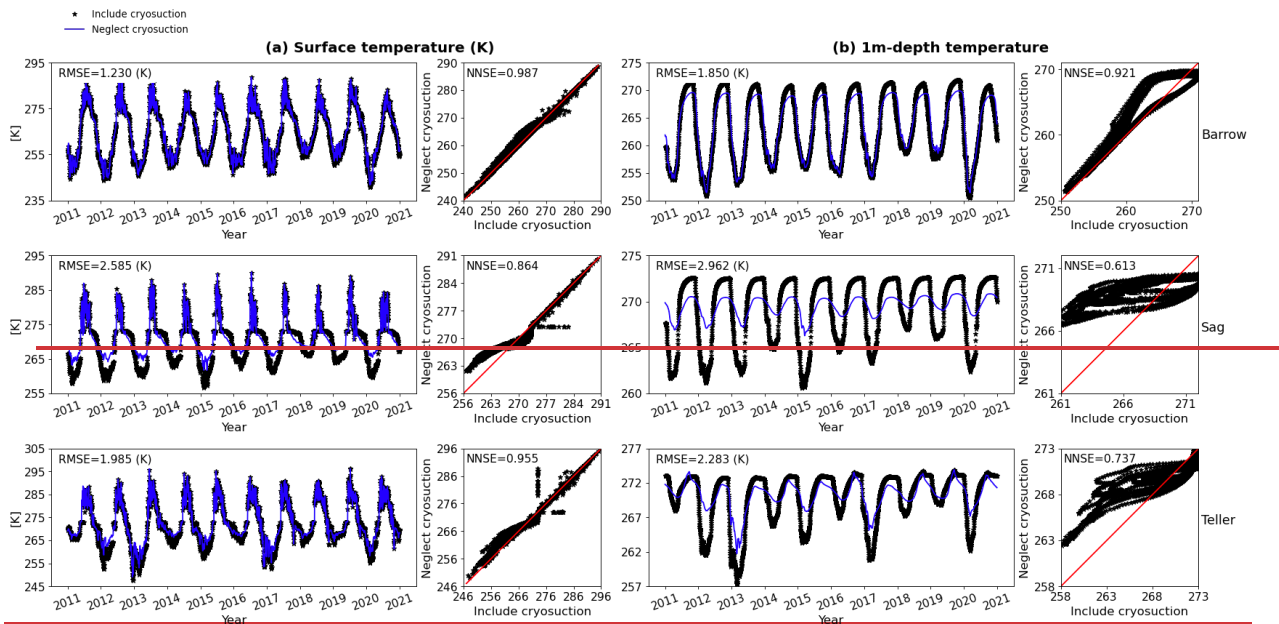


488  
489  
490

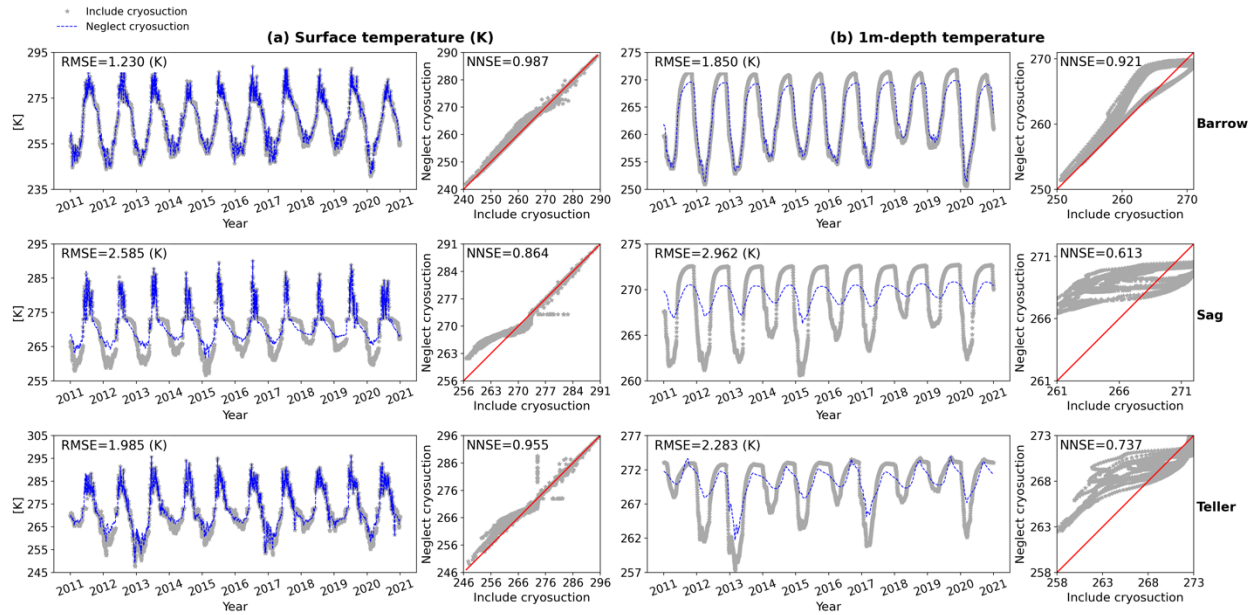
**Figure 7 Comparison of column simulations between including and neglecting cryosuction under conditions of Barrow, Sag, and Teller, in (a) thaw depth, (b) water saturation at 5 cm beneath surface.**

491 Finally, we also compared soil temperature obtained from models with or without cryosuction  
 492 ~~included; in-see~~ Figure 8. Surface temperature is little affected by cryosuction, except at the Sag  
 493 site, where the surface temperature is overestimated during winter. At 1 m depth, soil temperature  
 494 of Barrow is slightly changed in summer due to neglecting cryosuction. At both Sag and Teller,  
 495 the fluctuation range of temperature at 1 m beneath land surface is underestimated if the  
 496 cryosuction effect is not considered, especially at Sag, NNSE decreases to ~~0.6~~ approximately 0.6.  
 497 The reason that causes Sag and Teller are more sensitive to the effect of cryosuction on temperature  
 498 is associated with the larger water amount in the two sites. During freezing, soil freezes from  
 499 ground surface downward and from the bottom of active layer upward, forming a liquid zone in  
 500 between where the temperature approximates freezing point due to phase change (Figure S3.1(a)  
 501 in the Supplement shows an example of the column model under the Sag River condition at the  
 502 300<sup>th</sup> day of one year). Thus, this liquid zone isolates the upper permafrost from the soil surface  
 503 temperature variations due to the weakened conductive heat transport along the soil depth.  
 504 Additionally, the released latent heat in this liquid zone may retard soil freezing, which also tends  
 505 to reduce thermal conduction. However, cryosuction can speed up freezing and promote the  
 506 attenuation of the liquid zone (see S3.1(a) and (b) in Supplement. Figure S3.1(b) shows the  
 507 ice saturation at the same time with Figure S3.1(a), when the soil column still has large non-frozen  
 508 area), and thus decrease the impact of the liquid zone. Hence, the influence of cryosuction is more

509 significant with more soil water.  
 510 Therefore, from Figure 7 to Figure 9, neglecting cryosuction effect at column scale simulation has  
 511 less impact on integrated hydrological variables, but will cause significant difference when  
 512 estimating thaw depth and location-based variables. The difference among variables varies under  
 513 different climate conditions. Influence on integrated variables, such as evaporation and discharge,  
 514 are more obviously under warm and wet conditions (Teller); thaw depth and water saturation are  
 515 affected more under cold and low-rainfall conditions (Barrow); and soil temperature tends to be  
 516 influenced greater under cold and high precipitation (rain and snow) conditions (Sag).



517



518

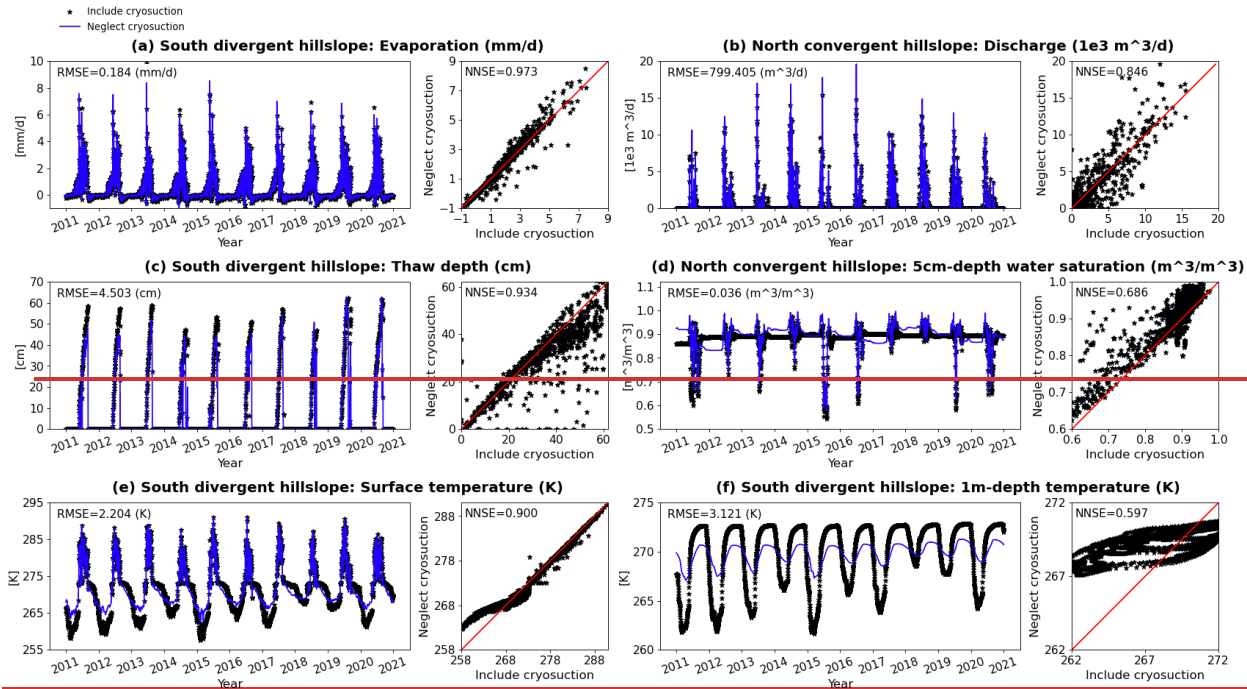
519 **Figure 8 Comparison of column simulations between including and neglecting cryosuction under conditions**  
 520 **of Barrow, Sag, and Teller, in (a) surface temperature, (b) temperature at 1 m beneath surface.**

521 Therefore, from Figure 6 to Figure 8, neglecting the cryosuction effect in column-scale simulations  
 522 has less impact on integrated hydrological metrics, but will cause significant difference when  
 523 estimating thaw depth and location-specific metrics. The difference among these metrics varies  
 524 under different climate conditions. Integrated metrics, such as evaporation and discharge, are  
 525 affected more under warm and wet conditions (Teller); thaw depth and water saturation are  
 526 affected more under cold and low-rainfall conditions (Barrow); and soil temperature tends to be  
 527 affected more under cold and high precipitation (rain and snow) conditions (Sag).

528 Neglecting soil cryosuction has a similar impact on hydrological outputs in hillslope scale models.

529 Figure 9 shows the comparison of the variables-metrics of interest discussed above under the Sag  
 530 climate. Evaporation, thaw depth, and temperature are presented based on south-facing divergent  
 531 hillslope models, while discharge and water saturation are from hillslope models with north-facing  
 532 convergent geometry. In general, neglecting soil cryosuction has a smaller effect on integrated  
 533 variables-metrics (evaporation and discharge) compared with other pointwise variables-metrics.  
 534 Though thaw depth presents a high NNSE of, approximately 0.94, and low RMSE of, about 4.5  
 535 cm compared to the average, indicating a good match between models considered and excluded  
 536 cryosuction, the estimation error during summer may reach as high as 10 cm, particularly from  
 537 2011 to 2017, as shown in Figure 9 (c). Obvious errors in water saturation and temperature, similar  
 538 with column-scale models, occur almost annually with respect to extrema during winter and

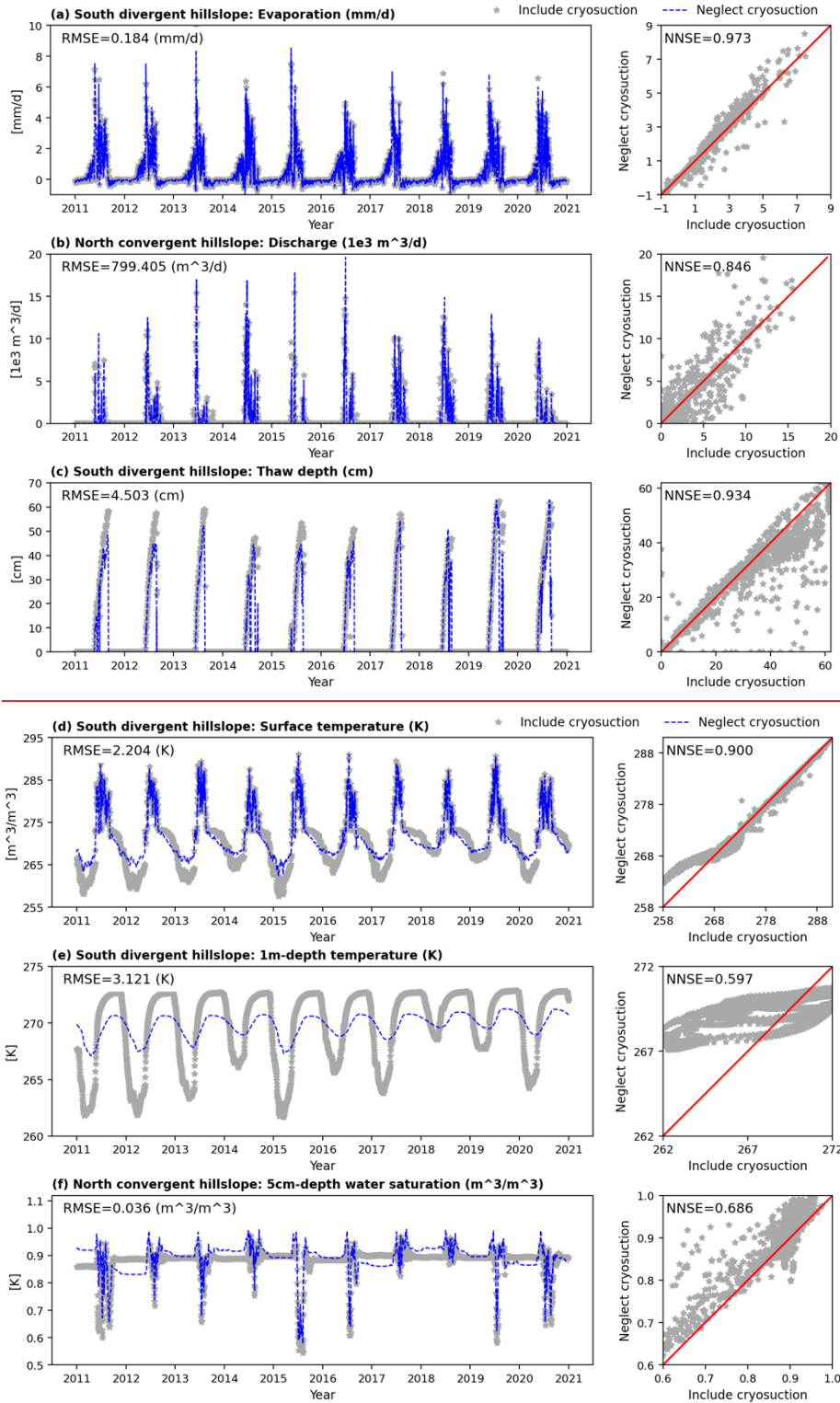
539 summer. Overall, compared to column-scale models, differences in evaporation, discharge, thaw  
 540 depth, and surface temperature due to neglecting cryosuction ~~effect~~ are relatively reduced at the  
 541 hillslope scale if comparing NNSEs (Table 5). Localized subsurface variables/metrics, such as  
 542 water saturation and 1m-depth soil temperature, show increased errors from column to hillslope  
 543 scale models, which is primarily caused by lateral flux exchange captured by hillslope modeling.



544



545



546

547

548

549

Figure 9 Comparison of hillslope simulations between including and neglecting cryosuction under conditions of Sag, in (a) evaporation, (b) discharge, (c) thaw depth, (d) water saturation at 5 cm beneath surface, (e) surface temperature, (f) temperature at 1 m beneath surface.



550  
551

**Table 5 NNSE of outputs from column and hillslope models under conditions of Sag shown in Figure 6 through Figure 9**

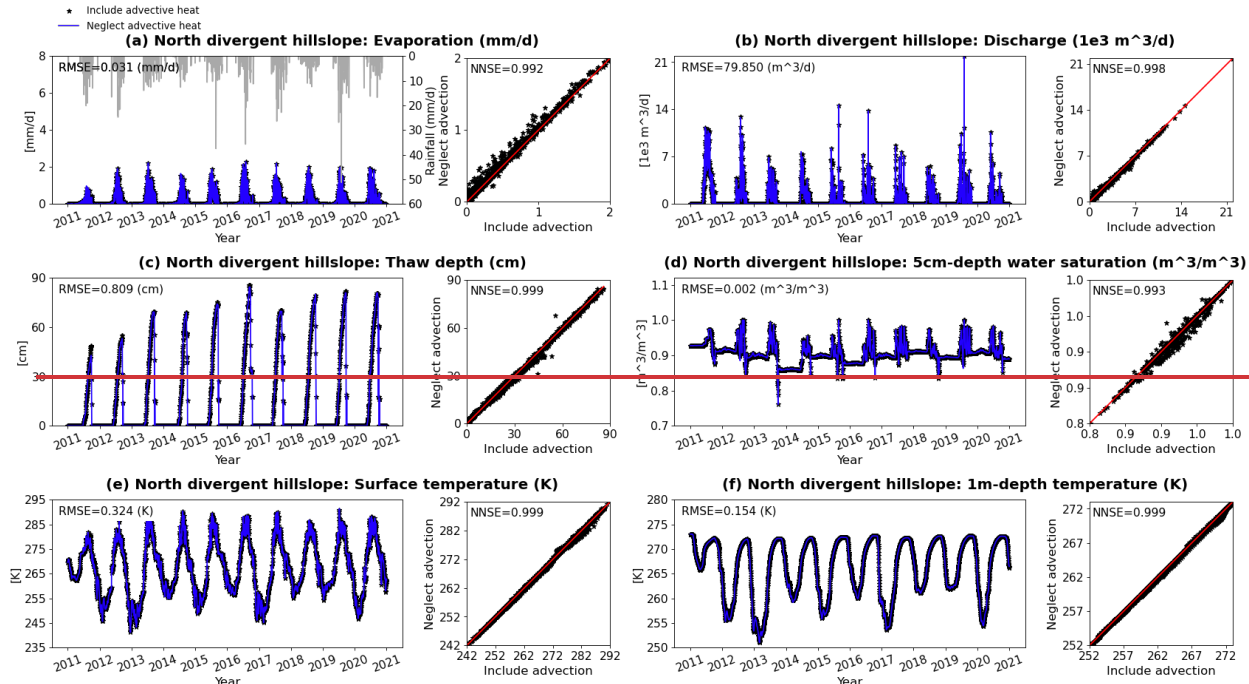
Scale	Evaporation (mm/d)	Discharge (m <sup>3</sup> /d)	Thaw depth (cm)	5cm-depth water saturation (-)	Surface temperature (K)	1m-depth temperature (K)
Column	0.936	0.631	0.904	0.926	0.864	0.613
Hillslope	0.973	0.846	0.934	0.686	0.900	0.597

552

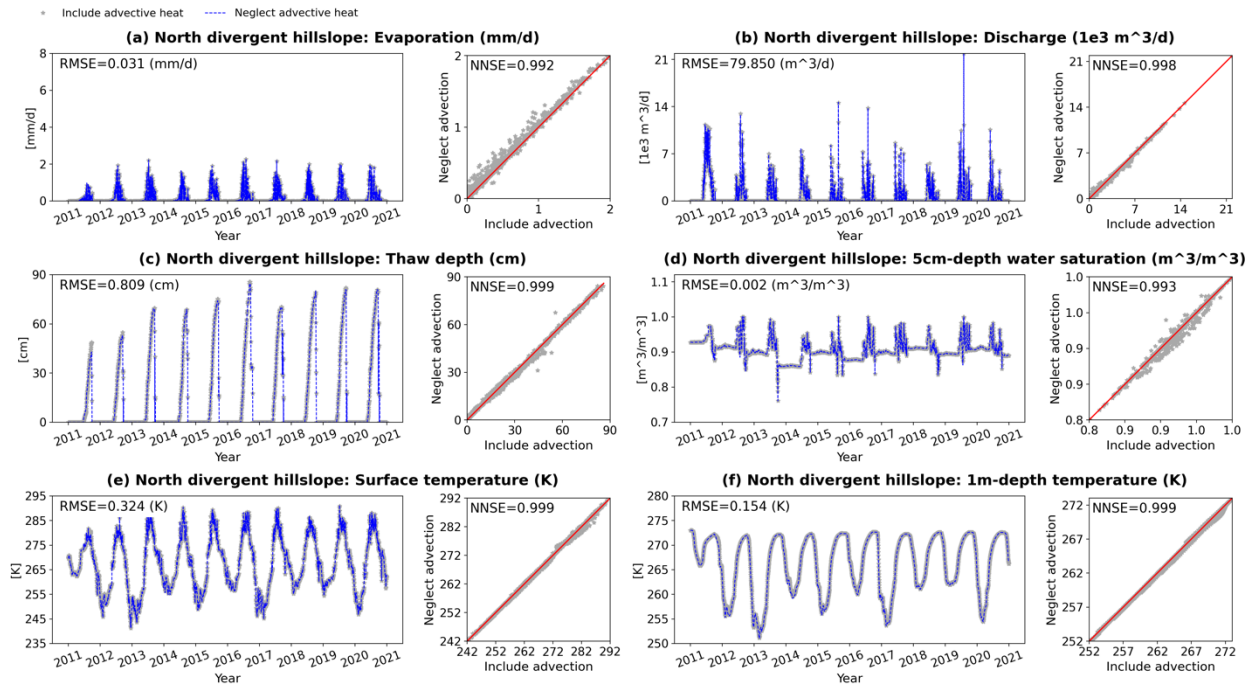
### 553 4.3 Advective heat transport

554 This section evaluates the performance of advective heat transport in modeling permafrost process.  
555 As above, we investigated the influence of neglecting heat advection on evaporation, discharge,  
556 thaw depth, total water saturation, and temperature. Overall, after comparing all hydrological  
557 outputs from models with different heat transport representations, heat advection is proved  
558 insignificant does not play a vital role in an normal Arctic system where the influence of localized  
559 groundwater flow can be neglected. after comparing all hydrological outputs from models with  
560 different heat transport representations. Comparisons based on column-scale and hillslope-scale  
561 models are not shown here (see Supplement); instead, the extreme case under conditions of Teller  
562 is presented (Figure 10). Teller is abundant in rainfall over the period of 2011-2020 (Figure 1). In  
563 the extreme case, evaporation was reduced factitiouslyartificially to almost a quarter of the original  
564 value (see Figure 6 (a) at Teller and Figure 10 (a)) for the purpose of increasing water flow rates.  
565 For instance, discharge has quadrupled after adjusting evaporation by comparing Figure 10 (b) and  
566 Figure 6 (b) at Teller. This specific scenario is chosen to maximize the potential effect of advective  
567 heat transport in a hillslope-scale Arctic system. Figure 10 illustrates comparisons on all outputs  
568 mentioned above from hillslope models without heat advection and with full thermal  
569 representation. Apparently, all RMSEs are extremely small, at least two orders of magnitude lower  
570 than the corresponding variable-metric average. Almost all NNSEs are approximately one, even  
571 for thaw depth, localized water saturation, and temperature. Under the assumption of large-scale  
572 Arctic systems ignoring the influence by localized groundwater flow features (e.g., ponds, gullies,  
573 etc.), the liquid water flux determines the advective heat transport in the subsurface. However, the  
574 flow velocity on average is quite low within the shallow active layer with limited thickness (see  
575 Figure S4.1 in Supplement). This result in that the advective heat transport only makes  
576 contributions within the top shallow layers, and the relatively larger advective heat flux is lower  
577 than the conductive heat flux over one order of magnitude (see Figure S4.2 in Supplement).

578 Therefore, for such large-scale Arctic systems where localized groundwater flow makes less  
 579 contributions, for most Arctic systems at this scale, it is reasonable to neglect advective heat  
 580 transport.



581



582

583 **Figure 10 Comparison of hillslope simulations between including and neglecting advective heat transport**  
 584 **under extreme conditions of Teller, in (a) evaporation, (b) discharge, (c) thaw depth, (d) water saturation at 5**  
 585 **cm beneath surface, (e) surface temperature, (f) temperature at 1 m beneath surface.**

586 In addition to simulated results, we also compared simulation times in percentage change between

587 hillslope models neglecting and including heat advection. ATS uses Algebraic Multigrid method  
 588 as preconditioner for solving, which has a relatively deficient performance in dealing with  
 589 hyperbolic equations. Thus, incorporating advective heat transport will aggravate computational  
 590 cost, particularly in case of both large spatial and temporal scale. Figure 12 shows the relative  
 591 percentage reduction in computational time for 10-year simulations after excluding heat advection  
 592 in both surface and subsurface thermal flux. It drops by 70%–80% under wet conditions (e.g.,  
 593 Sag and Teller) and 40%–60% under dry conditions (e.g., Barrow). Hence, neglecting advective  
 594 heat transport considerably improves the performance of large spatial temporal permafrost  
 595 hydrology simulations.



596  
 597 **Figure 12 Decreased percentage of simulation time after neglecting heat advection compared to full thermal**  
 598 **representation for all hillslope scale simulations.**

599 **4.4 Comprehensive comparison**

600 In the above three sections, we discussed time-series simulation comparisons. This section will  
 601 analyze the effect of equal ice-liquid density, neglecting cryosuction, and neglecting heat  
 602 advection on permafrost modeling outputs from holistic, average perspectives.

603 First, we extracted NNSEs of all variables—the metrics of interest obtained from all comparing  
 604 models for qualitative analysis. Table 6 shows an example based on column-scale models under  
 605 conditions of three different sites. Red numbers highlight the obviously reduced NNSEs of one or  
 606 two processes among the three for each variable/metric. Overall, neglecting advective heat  
 607 transport has the least influence on model outputs. Equal ice-liquid density primarily affects  
 608 saturation and has less effect on other variables/metrics. Excluding soil cryosuction makes the  
 609 greatest impact on almost all variables/metrics, especially in a relatively wet environment. Among  
 610 these metrics-variables, evaporation and surface temperature are less affected by the three physical  
 611 process representations, while location-based water saturation is most affected.

612 **Table 6 A summary of NNSEs of variables-metrics of interest obtained through column model comparison**

<b>Metrics</b>	<b>Barrow</b>			<b>Sag</b>			<b>Teller</b>		
	<i>Heat advection</i>	<i>Ice density</i>	<i>Cryosuction</i>	<i>Heat advection</i>	<i>Ice density</i>	<i>Cryosuction</i>	<i>Heat advection</i>	<i>Ice density</i>	<i>Cryosuction</i>
<u>Evaporation</u>	<u>0.997</u>	<u>0.994</u>	<u>0.899</u>	<u>0.993</u>	<u>0.992</u>	<u>0.937</u>	<u>0.999</u>	<u>0.996</u>	<u>0.903</u>
<u>Discharge</u>	<u>0.924</u>	<u>0.628</u>	<u>0.862</u>	<u>0.996</u>	<u>0.938</u>	<u>0.631</u>	<u>0.985</u>	<u>0.987</u>	<u>0.618</u>
<u>Thaw depth</u>	<u>0.997</u>	<u>0.996</u>	<u>0.852</u>	<u>0.991</u>	<u>0.979</u>	<u>0.904</u>	<u>0.997</u>	<u>0.989</u>	<u>0.952</u>
<u>5cm-depth <math>s_w</math></u>	<u>0.996</u>	<u>0.934</u>	<u>0.785</u>	<u>0.992</u>	<u>0.726</u>	<u>0.926</u>	<u>0.998</u>	<u>0.562</u>	<u>0.869</u>
<u>40cm-depth <math>s_w</math></u>	<u>0.993</u>	<u>0.022</u>	<u>0.213</u>	<u>0.995</u>	<u>0.062</u>	<u>0.311</u>	<u>0.999</u>	<u>0.281</u>	<u>0.850</u>
<u>Surface <math>T</math></u>	<u>1.000</u>	<u>1.000</u>	<u>0.987</u>	<u>0.999</u>	<u>0.999</u>	<u>0.864</u>	<u>1.000</u>	<u>1.000</u>	<u>0.955</u>
<u>1m-depth <math>T</math></u>	<u>1.000</u>	<u>1.000</u>	<u>0.921</u>	<u>1.000</u>	<u>1.000</u>	<u>0.613</u>	<u>1.000</u>	<u>0.999</u>	<u>0.737</u>

613

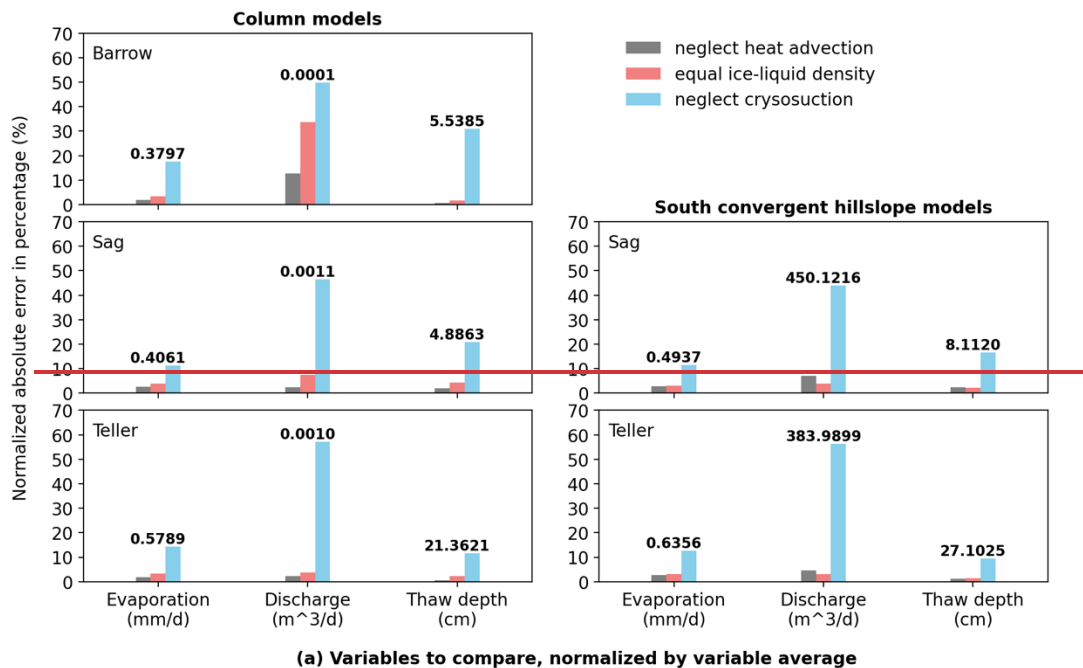
<b>Variables</b>	<b>Barrow</b>			<b>Sag</b>			<b>Teller</b>		
	<i>Heat advection</i>	<i>Ice density</i>	<i>Cryosuction</i>	<i>Heat advection</i>	<i>Ice density</i>	<i>Cryosuction</i>	<i>Heat advection</i>	<i>Ice density</i>	<i>Cryosuction</i>
<u>Evaporation</u>	<u>0.9971</u>	<u>0.9942</u>	<u>0.8991</u>	<u>0.9926</u>	<u>0.9917</u>	<u>0.9365</u>	<u>0.9989</u>	<u>0.9958</u>	<u>0.9033</u>
<u>Discharge</u>	<u>0.9235</u>	<u>0.6282</u>	<u>0.8615</u>	<u>0.9962</u>	<u>0.9377</u>	<u>0.6305</u>	<u>0.9854</u>	<u>0.9874</u>	<u>0.6175</u>
<u>Thaw depth</u>	<u>0.9970</u>	<u>0.9961</u>	<u>0.8517</u>	<u>0.9910</u>	<u>0.9791</u>	<u>0.9036</u>	<u>0.9969</u>	<u>0.9887</u>	<u>0.9524</u>
<u>5cm-depth <math>s_w</math></u>	<u>0.9959</u>	<u>0.9335</u>	<u>0.7851</u>	<u>0.9916</u>	<u>0.7260</u>	<u>0.9260</u>	<u>0.9979</u>	<u>0.5618</u>	<u>0.8690</u>
<u>40cm-depth <math>s_w</math></u>	<u>0.9932</u>	<u>0.0221</u>	<u>0.2130</u>	<u>0.9951</u>	<u>0.0622</u>	<u>0.3111</u>	<u>0.9990</u>	<u>0.2807</u>	<u>0.8498</u>
<u>Surface <math>T</math></u>	<u>0.9999</u>	<u>0.9999</u>	<u>0.9871</u>	<u>0.9993</u>	<u>0.9990</u>	<u>0.8642</u>	<u>0.9999</u>	<u>0.9996</u>	<u>0.9554</u>
<u>1m-depth <math>T</math></u>	<u>0.9999</u>	<u>0.9999</u>	<u>0.9207</u>	<u>0.9997</u>	<u>0.9996</u>	<u>0.6127</u>	<u>0.9997</u>	<u>0.9991</u>	<u>0.7366</u>

614 \*  $s_w$  and  $T$  in Table 6 are water saturation and temperature, respectively.

615 Furthermore, to quantitatively compare across the physical processes-quantitatively, we calculated  
616 the mean absolute error (MAE) for each variable-metric of interest over the simulation period of  
617 2011-2020. For evaporation, discharge, and thaw depth, the MAEs are normalized by the  
618 corresponding variable-metric average (numbers in Figure 11 (a)); for water saturation and  
619 temperature, the MAEs are normalized by their average annual fluctuation range (numbers in  
620 Figure 11 (b)). All normalized MAEs are presented in percentage, displayed in Figure 11 according  
621 to column- and hillslope-scale (e.g., south-facing convergent hillslope) models under three  
622 different climate conditions. Hillslope-scale model output under conditions of Barrow is not shown  
623 in that flat land occupies a majority of the area. A larger normalized MAE percentage indicates  
624 greater impact on the variable-metric resulted from a physical process.

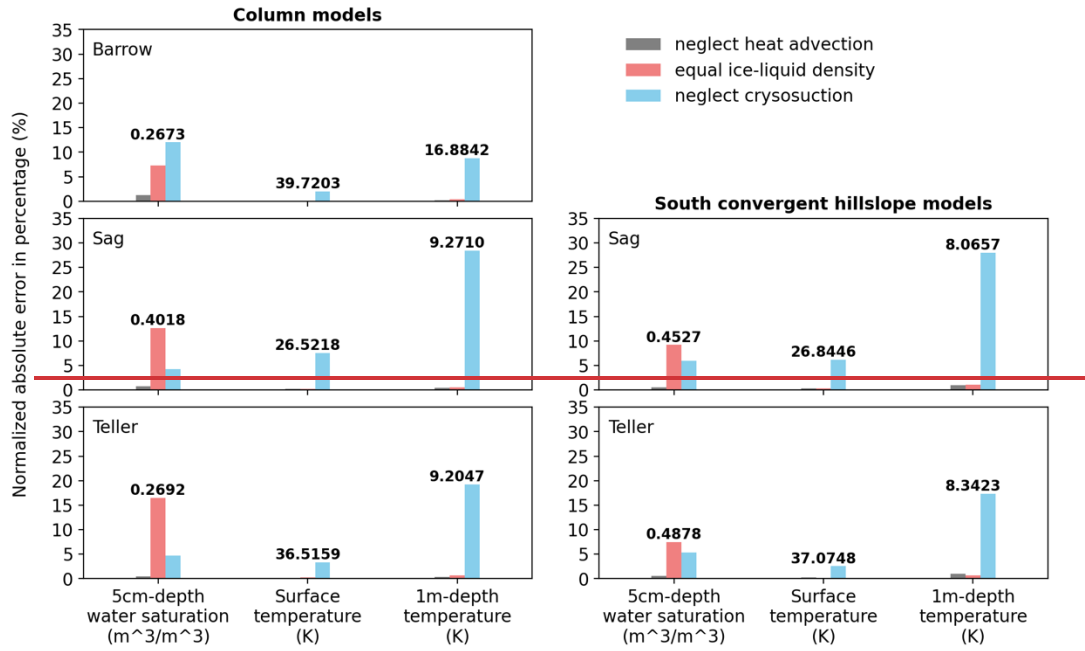
625 From the perspective of 10-year average, in general, each physical process of Arctic systems  
626 discussed in this paper presents a similar impact on variables-metrics between column and hillslope  
627 scales. Under climate and soil conditions of three different sites, neglecting cryosuction in  
628 permafrost modeling leads to the greatest influence on hydrological prediction amongst the three  
629 physical assumptions. As seen in Figure 11 (a), it will result in 10% ~ 20% deviation in evaporation,

630 50% ~ 60% in discharge, and 10% ~ 30% in thaw depth. Evaporation is the least affected among  
 631 the three variablesmetrics. Discharge is more affected in regions with abundant rainfall (Teller),  
 632 while in regions with less precipitation, evaporation and thaw depth are relatively affected  
 633 (Barrow). By comparison, assuming equal ice-liquid density and neglecting advective heat  
 634 transport may only cause 10% and 5% or even much lower error, respectively, in reference to the  
 635 annual average of a metricvariable. Specially in Barrow, models utilizing the same ice and liquid  
 636 densities and ignoring advective heat transport seem to make an obvious impact on discharge,  
 637 whereas this also results from its extremely low discharge (Figure 6 (b)).  
 638 Figure 11 (b) illustrates the normalized MAEs of water saturation at 5 cm beneath surface, as well  
 639 as temperature at surface and 1 m depth. The assumption of equal ice-liquid density primarily  
 640 affects the estimation of the water saturation profiles, which ~~it~~ can lead to about 5% ~ 15% error  
 641 relative to the annual change range, and the error percentage tends to slightly decrease when  
 642 applying hillslope-scale models due to the inclusion of lateral flow. Apart from this, neglecting  
 643 soil cryosuction still makes the largest impact. Surface temperature is the least affected variable  
 644 metric among all these model outputs even if cryosuction is not included in modeling. However,  
 645 at 1 m depth, error can increase to 10% ~ 30% by simulation without cryosuction representation.



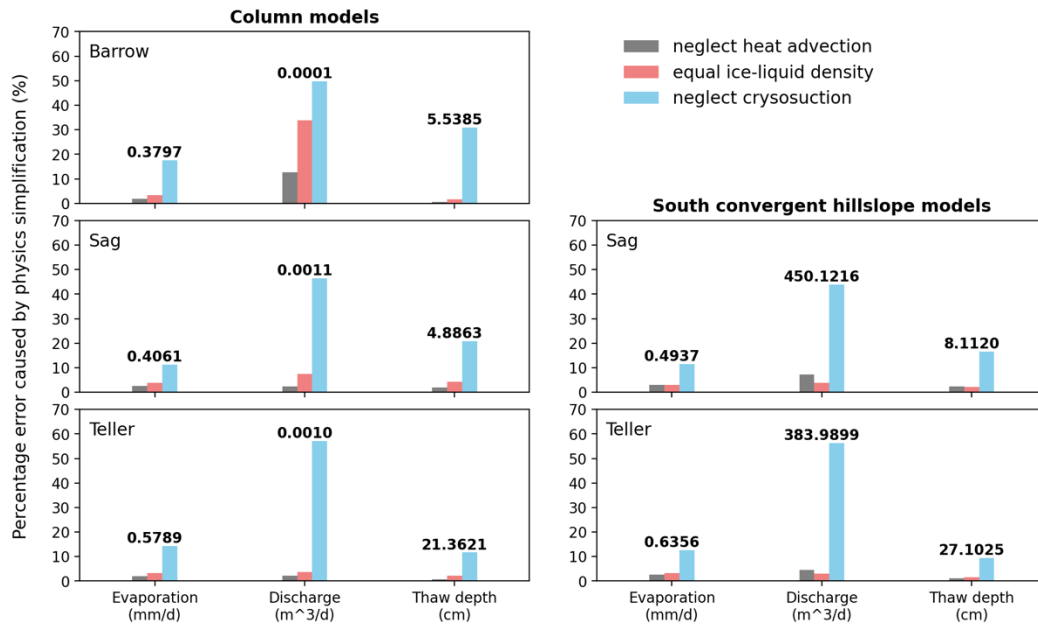
646  
647

648

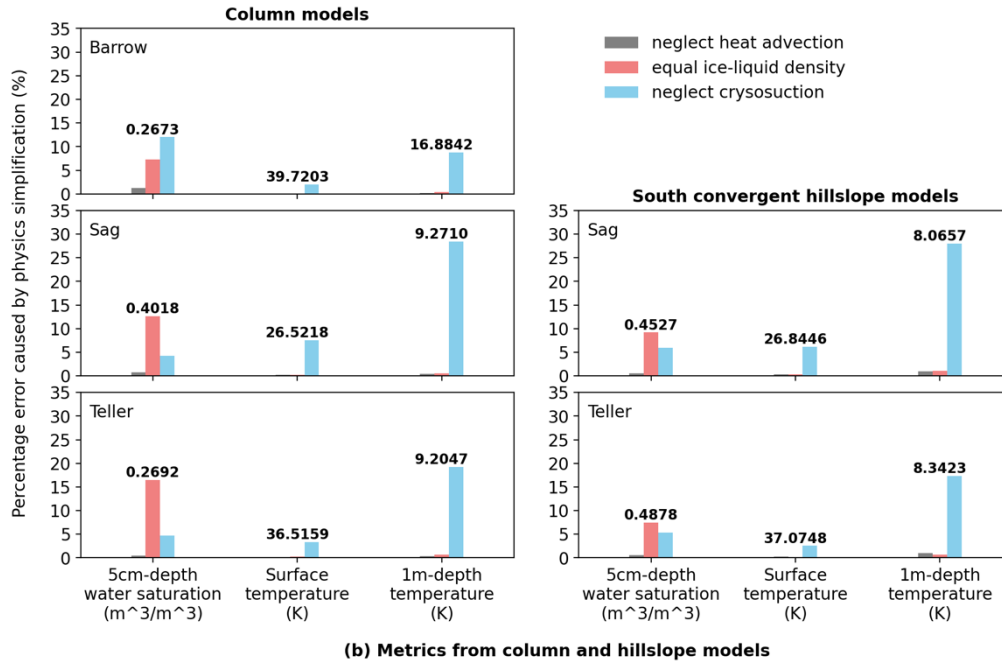


(b) Variables to compare, normalized by average annual fluctuation of variables

649



(a) Metrics from column and hillslope models



650

651 **Figure 11** Percentage errors for each metric caused by physics simplifications at column and hillslope scales.  
 652 **The percentage error refers to the averaged error of a metric over the period of 2011-2020 normalized by a**  
 653 **certain reference value obtained from full-physics model. Metrics include (a) evaporation, discharge, and**  
 654 **thaw depth; (b) water saturation, and temperatures. Numbers in figures are the corresponding reference**  
 655 **values for each metric: (a) 10-year average obtained from full-physics model; (b) 10-year averaged annual**  
 656 **fluctuation range obtained from full-physics model.**

## 657 5 Conclusion

658 [The premise of this study is, by starting from general mass and energy transport equations and](#)  
 659 [simplifying the process representations, we can use a process-rich model to understand the relative](#)  
 660 [importance of given process simplifications in describing permafrost hydrology. This process](#)  
 661 [sensitivity analysis, performed at the scale of field sites as opposed to previous studies at smaller](#)  
 662 [scales such as lab experiments, provides improved understanding in the processes governing](#)  
 663 [permafrost hydrology at this scale. As the simplifications considered here largely span the](#)  
 664 [equations considered in a class of process-rich models, this process sensitivity analysis is relevant](#)  
 665 [to model developers across a range of codes.](#)

666 Simplification of Arctic process representation is an essential consideration when developing  
 667 process-rich models for thermal permafrost hydrology. ~~There are following~~ three subsurface  
 668 process ~~simplificationses that~~ are commonly ~~described-applied in a simplified approach~~ for many  
 669 Arctic tundra models: (i) ice is prescribed the same density as liquid water; (ii) the effect of soil  
 670 cryosuction is neglected; (iii) advective heat transport is neglected. Here we investigated the



671 influence of these simplified representations on modeling field-scale permafrost hydrology in set  
672 of simplified geometries commonly used in the permafrost hydrology literature with the Advanced  
673 Terrestrial Simulator (ATS v1.2). We note that these conclusions are specific to conditions similar  
674 to these geometries, and should not be applied in cases where focusing flow mechanisms may  
675 dominate.

676 To do this, we conducted an ensemble of simulations ~~using the Advanced Terrestrial Simulator~~  
677 ~~(ATS v1.2)~~ to evaluate the impact of the above three process simplifications on field-scale  
678 predictions. The ensemble of simulations consisted of 62 numerical experiments considering  
679 various conditions, including different climate conditions and soil properties at three sites of  
680 Alaska, and different model scale conceptualizations. For evaluation, we compared integrated  
681 ~~variables-metrics~~ (evaporation, discharge), averaged thaw depth, and pointwise ~~variables-metrics~~  
682 (temperature, total water saturation), which are of general interest, among different models to  
683 assess the deviation of applying a simplified modeling assumption. The main conclusions, under  
684 the assumed conditions in ~~of~~ this study, are summarized as follows:

685 1) Excluding soil cryosuction ~~in permafrost models~~ can cause significant bias on estimation  
686 of in-most hydrological variables-metrics at field-scale permafrost simulations. Especially,  
687 according to-In particular, under the assumed condition this study, the average deviation  
688 in evaporation, discharge, and thaw depth may reach 10% ~ 20%, 50% ~ 60%, and 10% ~  
689 30%, respectively, relative to the corresponding annual average values. The prediction  
690 error for discharge may grow if rainfall rates increase. In the case of pointwise  
691 ~~variables-metrics~~, the error in temperature increases from a small amount at the surface up  
692 to 10% ~ 30% at 1 m beneath surface. The prediction of subsurface temperature and water  
693 saturation is especially affected when considering hillslope scale models. Therefore, soil  
694 cryosuction should be included when modeling permafrost change.

695 2) Assuming equal ice-liquid density will not result in especially large deviations when  
696 predicting most of the hydrological ~~variables-metrics~~, particularly at hillslope scales given  
697 all cases in this study. It primarily affects the prediction of the soil water saturation profile  
698 and can cause 5% ~ 15% error relative to the annual saturation fluctuation range. This  
699 difference may have consequences for the carbon cycle with regards to the production of  
700 methane versus carbon dioxide. Assigning liquid water density for ice may reduce  
701 computational time to a small extent in ATS, dependent on simulating conditions and

702 spatial and temporal scales.

703 3) For a large-scale ~~general~~ Arctic tundra system with limited localized groundwater flow  
704 features (e.g., taliks, thermo-erosion gullies, etc.), the prediction error in most ~~variables~~  
705 metrics of interest after neglecting advective heat transport is less than 5%, or even much  
706 lower. In the case of ATS, the simulation time cost for hillslope-scale models can decrease  
707 by 40% to 80% under conditions in this study. Ignoring heat advection in the absence of  
708 local, flow-focusing mechanisms, such as thermo-erosion gullies, seems a reasonable  
709 decision.

710 Through the comparison of permafrost hydrological outputs obtained from ensemble model setups  
711 targeted at the field scale, we confirm the importance and necessity of including soil cryosuction  
712 ~~effect~~ in predicting permafrost changes, and validate the application of equal ice-liquid density  
713 and neglecting advective heat transport for an general Arctic system where localized groundwater  
714 flow is not a dominant feature. The latter two may also ease computational cost dependent upon  
715 simulation conditions. We expect that this study can contribute to the development of permafrost  
716 hydrology models, as well as better selection of physical process representations for modelers, and  
717 better understanding of permafrost physics for the community.

## 718 Appendix

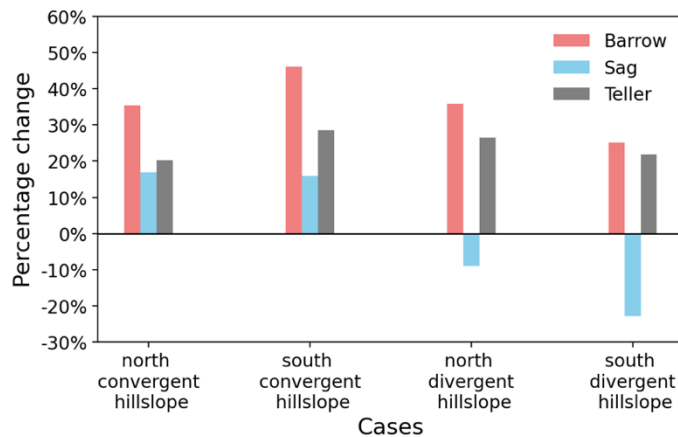
719 The following results may provide some information about computation cost for ATS users. In  
720 addition to the influence of process representations on permafrost hydrology metrics of general  
721 interest, we also investigated how much the simplified processes can affect the runtime of a model  
722 at the hillslope scale.

723 First, using the 10-year simulation with real ice density as references, the percentage change of  
724 time consumed after applying equal ice-liquid density was calculated and displayed in Figure A1.  
725 Overall, under the equal density assumption, it may take less time (positive values in figure), but  
726 no more than 25% and on average lower than 10%. However, the computation time may also  
727 increase (negative values in figure) under wet conditions, such as at Sag and Teller. Thus, given a  
728 long-period modeling of large-scale permafrost system, there is no consistent conclusion on  
729 whether equal ice-liquid density can ease computational cost. It depends on both the weather  
730 conditions and soil properties.



731  
 732 **Figure A1. The relative runtime change in percentage due to the assumption of equal ice-liquid density**  
 733 **compared to that with the real ice density representation for all hillslope scale models.**

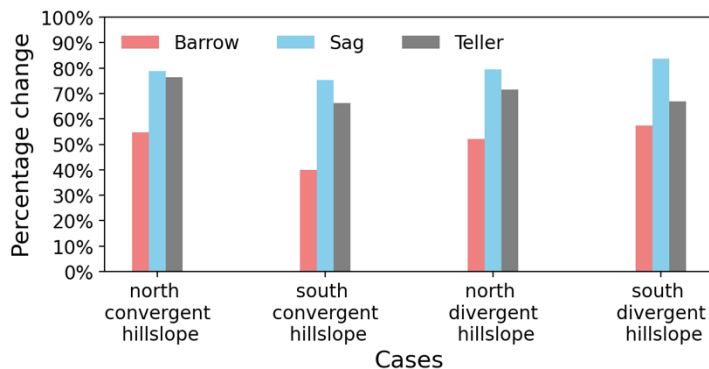
734 Second, section 4.2 has demonstrated that neglecting cryosuction will make a great impact on  
 735 hydrological estimations. As a significant physical process of permafrost, cryosuction should be  
 736 implemented in numerical models even if additional computation effort is potentially required.  
 737 However, based on the hillslope models we conducted, including cryosuction does not necessarily  
 738 raise computational cost, which also depends on specific soil properties and conditions. The cases  
 739 that consume more time after considering cryosuction effect just increase the time by 10% ~ 30%,  
 740 and less than 20% on average (see Figure A2).



741  
 742 **Figure A2. The relative runtime change in percentage after neglecting cryosuction compared to the cases with**  
 743 **cryosuction for all hillslope scale models.**

744 Third, in terms of heat advection, ATS uses the Algebraic Multigrid method as preconditioner for  
 745 solving, which has a relatively deficient performance in dealing with hyperbolic equations. Thus,  
 746 incorporating advective heat transport will aggravate computational cost, particularly in case of  
 747 both large spatial and temporal scales. Figure A3 shows the relative percentage reduction in  
 748 computational time for 10-year simulations after excluding heat advection in both surface and

749 subsurface thermal flux. It drops by 70% ~ 80% under wet conditions (e.g., Sag and Teller) and  
750 40% ~ 60% under dry conditions (e.g., Barrow). Hence, neglecting advective heat transport  
751 considerably improves the performance of large spatial-temporal permafrost hydrology  
752 simulations.



753 Figure A3. The relative runtime change in percentage due to the neglect of advective heat transport for all  
754 hillslope scale models.

#### 756 Code availability

757 Advanced Terrestrial Simulator (ATS) is an open-source code for solving ecosystem-based,  
758 integrated, distributed hydrology, and available at <https://github.com/amanzi/ats>. Simulations were  
759 conducted using version 1.2 (Coon et al., 2021).

#### 760 Data availability

761 Data sources of wind speed are cited in the text. The raw forcing data acquired from Daymet, the  
762 processed forcing data used for simulation, and simulation output data are available through  
763 [https://github.com/gaobhub/data\\_for\\_paper\\_model\\_comparison](https://github.com/gaobhub/data_for_paper_model_comparison).

#### 764 Author contributions

765 Bo Gao did some revision of the code to add options for process representations, designed  
766 numerical experiments and setup models, did data analysis and interpretation, drafted and revised  
767 the article. Ethan T. Coon implemented the code in which the study was done, conceptualized the  
768 study, helped debug the runs, and helped draft and revise the article.

#### 769 Competing interests

770 The authors declare that they have no conflict of interest.

## 771 **Acknowledgement**

772 Both authors are supported by the U.S. Department of Energy, Office of Science, Biological and  
773 Environmental Research program under the InteRFACE project. This research used resources of  
774 the Compute and Data Environment for Science (CADES) at the Oak Ridge National Laboratory,  
775 which is supported by the Office of Science of the U.S. Department of Energy under Contract No.  
776 DE-AC05-00OR22725.

## 777 **References**

778 Abolt, C. J., Young, M. H., Atchley, A. L., Harp, D. R., and Coon, E. T.: Feedbacks Between  
779 Surface Deformation and Permafrost Degradation in Ice Wedge Polygons, Arctic Coastal Plain,  
780 Alaska, *J. Geophys. Res. Earth Surf.*, 125, e2019JF005349, <https://doi.org/10.1029/2019JF005349>,  
781 2020.

782 Atchley, A. L., Painter, S. L., Harp, D. R., Coon, E. T., Wilson, C. J., Liljedahl, A. K., and  
783 Romanovsky, V. E.: Using field observations to inform thermal hydrology models of permafrost  
784 dynamics with ATS (v0.83), *Geosci. Model Dev.*, 8, 2701–2722, [https://doi.org/10.5194/gmd-8-](https://doi.org/10.5194/gmd-8-2701-2015)  
785 2701-2015, 2015.

786 Berteaux, D., Gauthier, G., Domine, F., Ims, R. A., Lamoureux, S. F., Lévesque, E., and Yoccoz,  
787 N.: Effects of changing permafrost and snow conditions on tundra wildlife: critical places and  
788 times, *Arct. Sci.*, 3, 65–90, <https://doi.org/10.1139/as-2016-0023>, 2017.

789 Bui, M. T., Lu, J., and Nie, L.: A Review of Hydrological Models Applied in the Permafrost-  
790 Dominated Arctic Region, *Geosciences*, 10, 401, <https://doi.org/10.3390/geosciences10100401>,  
791 2020.

792 Busey, B., Bolton, B., Wilson, C., and Cohen, L.: Surface Meteorology at Teller Site Stations,  
793 Seward Peninsula, Alaska, Ongoing from 2016, 2017.

794 Chen, L., Fortier, D., McKenzie, J. M., and Sliger, M.: Impact of heat advection on the thermal  
795 regime of roads built on permafrost, *Hydrol. Process.*, 34, 1647–1664,  
796 <https://doi.org/10.1002/hyp.13688>, 2020.

797 Cheng, G. and Wu, T.: Responses of permafrost to climate change and their environmental  
798 significance, Qinghai-Tibet Plateau, *J. Geophys. Res. Earth Surf.*, 112,  
799 <https://doi.org/10.1029/2006JF000631>, 2007.

800 Coon, E. T., David Moulton, J., and Painter, S. L.: Managing complexity in simulations of land  
801 surface and near-surface processes, *Environ. Model. Softw.*, 78, 134–149,

802 <https://doi.org/10.1016/j.envsoft.2015.12.017>, 2016.

803 Coon, E. T., Moulton, J. D., Kikinzon, E., Berndt, M., Manzini, G., Garimella, R., Lipnikov, K.,  
804 and Painter, S. L.: Coupling surface flow and subsurface flow in complex soil structures using  
805 mimetic finite differences, *Adv. Water Resour.*, 144, 103701,  
806 <https://doi.org/10.1016/j.advwatres.2020.103701>, 2020.

807 Dagenais, S., Molson, J., Lemieux, J.-M., Fortier, R., and Therrien, R.: Coupled cryo-  
808 hydrogeological modelling of permafrost dynamics near Umiujaq (Nunavik, Canada), *Hydrogeol.*  
809 *J.*, 28, 887–904, <https://doi.org/10.1007/s10040-020-02111-3>, 2020.

810 Dall’Amico, M., Endrizzi, S., Gruber, S., and Rigon, R.: A robust and energy-conserving model  
811 of freezing variably-saturated soil, *The Cryosphere*, 5, 469–484, [https://doi.org/10.5194/tc-5-469-](https://doi.org/10.5194/tc-5-469-2011)  
812 2011, 2011.

813 Dearborn, K. D., Wallace, C. A., Patankar, R., and Baltzer, J. L.: Permafrost thaw in boreal  
814 peatlands is rapidly altering forest community composition, *J. Ecol.*, 109, 1452–1467,  
815 <https://doi.org/10.1111/1365-2745.13569>, 2021.

816 Devoie, É. G. and Craig, J. R.: A Semianalytical Interface Model of Soil Freeze/Thaw and  
817 Permafrost Evolution, *Water Resour. Res.*, 56, e2020WR027638,  
818 <https://doi.org/10.1029/2020WR027638>, 2020.

819 Endrizzi, S., Gruber, S., Dall’Amico, M., and Rigon, R.: GEOtop 2.0: simulating the combined  
820 energy and water balance at and below the land surface accounting for soil freezing, snow cover  
821 and terrain effects, *Geosci. Model Dev.*, 7, 2831–2857, <https://doi.org/10.5194/gmd-7-2831-2014>,  
822 2014.

823 Fortier, D., Allard, M., and Shur, Y.: Observation of rapid drainage system development by  
824 thermal erosion of ice wedges on Bylot Island, Canadian Arctic Archipelago, *Permafr. Periglac.*  
825 *Process.*, 18, 229–243, <https://doi.org/10.1002/ppp.595>, 2007.

826 Godin, E., Fortier, D., and Coulombe, S.: Effects of thermo-erosion gullyng on hydrologic flow  
827 networks, discharge and soil loss, *Environ. Res. Lett.*, 9, 105010, [https://doi.org/10.1088/1748-](https://doi.org/10.1088/1748-9326/9/10/105010)  
828 9326/9/10/105010, 2014.

829 Gottardi, G. and Venutelli, M.: A control-volume finite-element model for two-dimensional  
830 overland flow, *Adv. Water Resour.*, 16, 277–284, [https://doi.org/10.1016/0309-1708\(93\)90019-C](https://doi.org/10.1016/0309-1708(93)90019-C),  
831 1993.

832 Grenier, C., Anbergen, H., Bense, V., Chanzy, Q., Coon, E., Collier, N., Costard, F., Ferry, M.,  
833 Frampton, A., Frederick, J., Gonçalves, J., Holmén, J., Jost, A., Kokh, S., Kurylyk, B., McKenzie,  
834 J., Molson, J., Mouche, E., Orgogozo, L., Pannetier, R., Rivière, A., Roux, N., Rühaak, W.,  
835 Scheidegger, J., Selroos, J.-O., Therrien, R., Vidstrand, P., and Voss, C.: Groundwater flow and  
836 heat transport for systems undergoing freeze-thaw: Intercomparison of numerical simulators for  
837 2D test cases, *Adv. Water Resour.*, 114, 196–218, <https://doi.org/10.1016/j.advwatres.2018.02.001>,  
838 2018.

- 839 Harp, D. R., Zlotnik, V., Abolt, C. J., Busey, B., Avendaño, S. T., Newman, B. D., Atchley, A. L.,  
840 Jafarov, E., Wilson, C. J., and Bennett, K. E.: New insights into the drainage of inundated ice-  
841 wedge polygons using fundamental hydrologic principles, *The Cryosphere*, 15, 4005–4029,  
842 <https://doi.org/10.5194/tc-15-4005-2021>, 2021.
- 843 Hinzman, L., Busey, B., Cable, W., and Romanovsky, V.: Surface Meteorology, Utqiagvik  
844 (Barrow), Alaska, Area A, B, C and D, Ongoing from 2012, 2014.
- 845 Hjort, J., Karjalainen, O., Aalto, J., Westermann, S., Romanovsky, V. E., Nelson, F. E.,  
846 Eitzelmüller, B., and Luoto, M.: Degrading permafrost puts Arctic infrastructure at risk by mid-  
847 century, *Nat. Commun.*, 9, 5147, <https://doi.org/10.1038/s41467-018-07557-4>, 2018.
- 848 Hugelius, G., Strauss, J., Zubrzycki, S., Harden, J. W., Schuur, E. a. G., Ping, C.-L., Schirrmeister,  
849 L., Grosse, G., Michaelson, G. J., Koven, C. D., O'Donnell, J. A., Elberling, B., Mishra, U., Camill,  
850 P., Yu, Z., Palmtag, J., and Kuhry, P.: Estimated stocks of circumpolar permafrost carbon with  
851 quantified uncertainty ranges and identified data gaps, *Biogeosciences*, 11, 6573–6593,  
852 <https://doi.org/10.5194/bg-11-6573-2014>, 2014.
- 853 Jafarov, E. E., Coon, E. T., Harp, D. R., Wilson, C. J., Painter, S. L., Atchley, A. L., and  
854 Romanovsky, V. E.: Modeling the role of preferential snow accumulation in through talik  
855 development and hillslope groundwater flow in a transitional permafrost landscape, *Environ. Res.*  
856 *Lett.*, 13, 105006, <https://doi.org/10.1088/1748-9326/aadd30>, 2018.
- 857 Jan, A., Coon, E. T., Painter, S. L., Garimella, R., and Moulton, J. D.: An intermediate-scale model  
858 for thermal hydrology in low-relief permafrost-affected landscapes, *Comput. Geosci.*, 22, 163–  
859 177, <https://doi.org/10.1007/s10596-017-9679-3>, 2018.
- 860 Jan, A., Coon, E. T., and Painter, S. L.: Evaluating integrated surface/subsurface permafrost  
861 thermal hydrology models in ATS (v0.88) against observations from a polygonal tundra site,  
862 *Geosci. Model Dev.*, 13, 2259–2276, <https://doi.org/10.5194/gmd-13-2259-2020>, 2020.
- 863 Jorgenson, M. T., Racine, C. H., Walters, J. C., and Osterkamp, T. E.: Permafrost Degradation and  
864 Ecological Changes Associated with a Warming Climate in Central Alaska, *Clim. Change*, 48,  
865 551–579, <https://doi.org/10.1023/A:1005667424292>, 2001.
- 866 Karra, S., Painter, S. L., and Lichtner, P. C.: Three-phase numerical model for subsurface  
867 hydrology in permafrost-affected regions (PFLOTRAN-ICE v1.0), *The Cryosphere*, 8, 1935–1950,  
868 <https://doi.org/10.5194/tc-8-1935-2014>, 2014.
- 869 Kurylyk, B. L. and Watanabe, K.: The mathematical representation of freezing and thawing  
870 processes in variably-saturated, non-deformable soils, *Adv. Water Resour.*, 60, 160–177,  
871 <https://doi.org/10.1016/j.advwatres.2013.07.016>, 2013.
- 872 Kurylyk, B. L., MacQuarrie, K. T. B., and McKenzie, J. M.: Climate change impacts on  
873 groundwater and soil temperatures in cold and temperate regions: Implications, mathematical  
874 theory, and emerging simulation tools, *Earth-Sci. Rev.*, 138, 313–334,  
875 <https://doi.org/10.1016/j.earscirev.2014.06.006>, 2014.



876 Liu, W., Fortier, R., Molson, J., and Lemieux, J.-M.: Three-Dimensional Numerical Modeling of  
877 Cryo-Hydrogeological Processes in a River-Talik System in a Continuous Permafrost  
878 Environment, *Water Resour. Res.*, 58, e2021WR031630, <https://doi.org/10.1029/2021WR031630>,  
879 2022.

880 Luethi, R., Phillips, M., and Lehning, M.: Estimating Non-Conductive Heat Flow Leading to Intra-  
881 Permafrost Talik Formation at the Ritigraben Rock Glacier (Western Swiss Alps), *Permafr.*  
882 *Periglac. Process.*, 28, 183–194, <https://doi.org/10.1002/ppp.1911>, 2017.

883 McKenzie, J. M. and Voss, C. I.: Permafrost thaw in a nested groundwater-flow system, *Hydrogeol.*  
884 *J.*, 21, 299–316, <https://doi.org/10.1007/s10040-012-0942-3>, 2013.

885 McKenzie, J. M., Voss, C. I., and Siegel, D. I.: Groundwater flow with energy transport and water-  
886 ice phase change: numerical simulations, benchmarks, and application to freezing in peat bogs,  
887 *Adv. Water Resour.*, 30, 966–983, <https://doi.org/10.1016/j.advwatres.2006.08.008>, 2007.

888 NEON (National Ecological Observatory Network): 2D wind speed and direction  
889 (DP1.00001.001): RELEASE-2021, 2021.

890 Noh, J.-H., Lee, S.-R., and Park, H.: Prediction of cryo-SWCC during freezing based on pore-size  
891 distribution, *Int. J. Geomech.*, 12, 428–438, [https://doi.org/10.1061/\(ASCE\)GM.1943-5622.0000134](https://doi.org/10.1061/(ASCE)GM.1943-5622.0000134), 2012.

893 O'Connor, M. T., Cardenas, M. B., Ferencz, S. B., Wu, Y., Neilson, B. T., Chen, J., and Kling, G.  
894 W.: Empirical Models for Predicting Water and Heat Flow Properties of Permafrost Soils,  
895 *Geophys. Res. Lett.*, 47, e2020GL087646, <https://doi.org/10.1029/2020GL087646>, 2020.

896 Painter, S. L.: Three-phase numerical model of water migration in partially frozen geological  
897 media: model formulation, validation, and applications, *Comput. Geosci.*, 15, 69–85,  
898 <https://doi.org/10.1007/s10596-010-9197-z>, 2011.

899 Painter, S. L. and Karra, S.: Constitutive Model for Unfrozen Water Content in Subfreezing  
900 Unsaturated Soils, *Vadose Zone J.*, 13, vzj2013.04.0071, <https://doi.org/10.2136/vzj2013.04.0071>,  
901 2014.

902 Painter, S. L., Coon, E. T., Atchley, A. L., Berndt, M., Garimella, R., Moulton, J. D., Svyatskiy,  
903 D., and Wilson, C. J.: Integrated surface/subsurface permafrost thermal hydrology: Model  
904 formulation and proof-of-concept simulations: integrated permafrost thermal hydrology, *Water*  
905 *Resour. Res.*, 52, 6062–6077, <https://doi.org/10.1002/2015WR018427>, 2016.

906 Ren, J., Vanapalli, S., and Han, Z.: Soil freezing process and different expressions for the soil-  
907 freezing characteristic curve, *Sci. Cold Arid Reg.*, 9, 221–228,  
908 <https://doi.org/10.3724/SP.J.1226.2017.00221>, 2017.

909 Riseborough, D., Shiklomanov, N., Etzelmüller, B., Gruber, S., and Marchenko, S.: Recent  
910 advances in permafrost modelling, *Permafr. Periglac. Process.*, 19, 137–156,  
911 <https://doi.org/10.1002/ppp.615>, 2008.

- 912 Rowland, J. C., Travis, B. J., and Wilson, C. J.: The role of advective heat transport in talik  
913 development beneath lakes and ponds in discontinuous permafrost, *Geophys. Res. Lett.*, 38,  
914 <https://doi.org/10.1029/2011GL048497>, 2011.
- 915 Sjöberg, Y., Coon, E., K. Sannel, A. B., Pannetier, R., Harp, D., Frampton, A., Painter, S. L., and  
916 Lyon, S. W.: Thermal effects of groundwater flow through subarctic fens: A case study based on  
917 field observations and numerical modeling, *Water Resour. Res.*, 52, 1591–1606,  
918 <https://doi.org/10.1002/2015WR017571>, 2016.
- 919 Stuurop, J. C., van der Zee, S. E. A. T. M., Voss, C. I., and French, H. K.: Simulating water and  
920 heat transport with freezing and cryosuction in unsaturated soil: Comparing an empirical, semi-  
921 empirical and physically-based approach, *Adv. Water Resour.*, 149, 103846,  
922 <https://doi.org/10.1016/j.advwatres.2021.103846>, 2021.
- 923 Sugimoto, A., Yanagisawa, N., Naito, D., Fujita, N., and Maximov, T. C.: Importance of  
924 permafrost as a source of water for plants in east Siberian taiga, *Ecol. Res.*, 17, 493–503,  
925 <https://doi.org/10.1046/j.1440-1703.2002.00506.x>, 2002.
- 926 Tesi, T., Muschitiello, F., Smittenberg, R. H., Jakobsson, M., Vonk, J. E., Hill, P., Andersson, A.,  
927 Kirchner, N., Noormets, R., Dudarev, O., Semiletov, I., and Gustafsson, Ö.: Massive  
928 remobilization of permafrost carbon during post-glacial warming, *Nat. Commun.*, 7, 13653,  
929 <https://doi.org/10.1038/ncomms13653>, 2016.
- 930 Thornton, M. M., Wei, Y., Thornton, P. E., Shrestha, R., Kao, S., and Wilson, B. E.: Daymet:  
931 Station-Level Inputs and Cross-Validation Result for North America, Version 4, 2020.
- 932 Thornton, P. E., Shrestha, R., Thornton, M., Kao, S.-C., Wei, Y., and Wilson, B. E.: Gridded daily  
933 weather data for North America with comprehensive uncertainty quantification, *Sci. Data*, 8, 190,  
934 <https://doi.org/10.1038/s41597-021-00973-0>, 2021.
- 935 Van Genuchten, M. T.: A Closed-form Equation for Predicting the Hydraulic Conductivity of  
936 Unsaturated Soils, *Soil Sci. Soc. Am. J.*, 44, 892–898,  
937 <https://doi.org/10.2136/sssaj1980.03615995004400050002x>, 1980.
- 938 Viterbo, P., Beljaars, A., Mahfouf, J.-F., and Teixeira, J.: The representation of soil moisture  
939 freezing and its impact on the stable boundary layer, *Q. J. R. Meteorol. Soc.*, 125, 2401–2426,  
940 <https://doi.org/10.1002/qj.49712555904>, 1999.
- 941 Walvoord, M. A. and Kurylyk, B. L.: Hydrologic Impacts of Thawing Permafrost—A Review,  
942 *Vadose Zone J.*, 15, <https://doi.org/10.2136/vzj2016.01.0010>, 2016.
- 943 Wasantha Lal, A. M.: Weighted Implicit Finite-Volume Model for Overland Flow, *J. Hydraul.*  
944 *Eng.*, 124, 941–950, [https://doi.org/10.1061/\(ASCE\)0733-9429\(1998\)124:9\(941\)](https://doi.org/10.1061/(ASCE)0733-9429(1998)124:9(941)), 1998.
- 945 Weismüller, J., Wollschläger, U., Boike, J., Pan, X., Yu, Q., and Roth, K.: Modeling the thermal  
946 dynamics of the active layer at two contrasting permafrost sites on Svalbard and on the Tibetan  
947 Plateau, *The Cryosphere*, 5, 741–757, <https://doi.org/10.5194/tc-5-741-2011>, 2011.

948 Westermann, S., Langer, M., Boike, J., Heikenfeld, M., Peter, M., Etzelmüller, B., and Krinner,  
949 G.: Simulating the thermal regime and thaw processes of ice-rich permafrost ground with the land-  
950 surface model CryoGrid 3, *Geosci. Model Dev.*, 9, 523–546, <https://doi.org/10.5194/gmd-9-523->  
951 2016, 2016.

952 Zhang, T., Barry, R. G., Knowles, K., Heginbottom, J. A., and Brown, J.: Statistics and  
953 characteristics of permafrost and ground-ice distribution in the Northern Hemisphere, *Polar Geogr.*,  
954 31, 47–68, <https://doi.org/10.1080/10889370802175895>, 2008.

955